

TECHNICAL REPORT STANDARD PAGE

1. Report No. FHWA/LA. 13/520		2. Government Accession No.	3. Recipient's Catalog No.
4. Title and Subtitle Field Demonstration of New Bridge Approach Slab Designs and Performance		5. Report Date June 2014	
		6. Performing Organization Code LTRC Project Number: 05-1GT SIO Number: 30000116	
7. Author(s) Murad Y. Abu-Farsakh, Ph.D., P.E., and Qiming Chen, Ph.D., P.E.		8. Performing Organization Report No.	
9. Performing Organization Name and Address Louisiana Transportation Research Center 4101 Gourrier Avenue Baton Rouge, LA 70808		10. Work Unit No.	
		11. Contract or Grant No. LTRC Number: 05-1GT SIO Number: 30000116	
12. Sponsoring Agency Name and Address Louisiana Transportation Research Center 4101 Gourrier Avenue Baton Rouge, LA 70808		13. Type of Report and Period Covered Final Report July 2009 - August 2013	
		14. Sponsoring Agency Code	
15. Supplementary Notes Conducted in Cooperation with the U.S. Department of Transportation, Federal Highway Administration			
16. Abstract The Louisiana Department of Transportation and Development (DOTD) has initiated a major effort to minimize the bridge end bump problem associated with differential settlement. As a result, a new design for the approach slab was proposed, which requires increasing the slab flexural rigidity (EI), and using reinforced soil foundation (RSF) to support the slab and traffic loads at the roadway pavement/approach slab joint (R/S joint). Reinforcing the soil underneath the strip footing will result in increasing the soil's bearing capacity and reducing the embankment settlement by redistributing the loads imposed by the slab and traffic over a wider area. Bayou Courtableau Bridge was selected as a demonstration project to evaluate, validate, and verify the new bridge approach slab design method proposed in a previous study. The east and west approach slabs at Bayou Courtableau Bridge are 40 ft. long by 40 ft. wide. The west approach slab was designed using the proposed new method with slab thickness of 16 in., while the east approach slab was designed using the traditional method with slab thickness of 12 in. The pavement end side of the approach slab was supported by a 4.0-ft. wide strip footing with the soil underneath it reinforced by six layers of geogrid placed at a vertical spacing of 12 in. The geosynthetic reinforced soil below the strip footing was designed according to the methodology proposed in previous study. The west approach slab was instrumented with pressure cells to measure the pressure distribution underneath the footing and contact pressure underneath the slabs. Strain gauges were used to measure strain distribution along geogrid reinforcement and sister-bar strain gauges to measure strains within the slab. The east approach slab was instrumented with pressure cells to measure the contact pressure underneath slab. Two static load tests were conducted on both the west and east approach slabs at two different times after construction. The performance of the approach slabs, including deformation and internal stresses of concrete slab, contact stresses between slab and embankment, stress distributions within reinforced soil foundation, and strain distributions along the geogrid, was monitored during the tests. The test results indicated that the west approach slab (with new design) lost most of its supports from the soil; while the east approach slab (with traditional design) kept losing its contacts from the soil starting from the bridge side towards the pavement side after about a year and half. The roughness profiles show better performance of the new approach slab system with much lower International Roughness Index (IRI) values. The year and a half monitoring program at Bayou Courtableau Bridge demonstrated much better performance of the new approach slab design system (west approach slab) compared to the traditional design. The magnitude and rate of embankment settlement at Bayou Courtableau Bridge site was also monitored (for the two embankment sides) during and after the construction, and the results were compared with the laboratory calculated settlements and the piezocone penetration test (PCPT)-based settlement prediction methods. The results showed better predictions using PCPT methods as compared to laboratory results.			
17. Key Words		18. Distribution Statement Unrestricted. This document is available through the National Technical Information Service, Springfield, VA 21161.	
19. Security Classif. (of this report) Unclassified	20. Security Classif. (of this page) Unclassified	21. No. of Pages 71	22. Price

Project Review Committee

Each research project will have an advisory committee appointed by the LTRC Director. The Project Review Committee is responsible for assisting the LTRC Administrator or Manager in the development of acceptable research problem statements, requests for proposals, review of research proposals, oversight of approved research projects, and implementation of findings.

The dedication and work effort of the following Project Review Committee members to guide this research study to fruition are acknowledged and appreciated.

LTRC Administrator

Zhongjie “Doc” Zhang, Ph.D., P.E.
Pavement and Geotechnical Research Administrator

Members

Steve Meunier, DOTD
Arthur D’Andrea, DOTD
Chris Nickel, DOTD
Ching Tsai, DOTD
Jenny Fu, DOTD
Arturo Aguirre, FHWA

Directorate Implementation Sponsor

Richard Savoie, DOTD Chief Engineer

Field Demonstration of New Bridge Approach Slab Designs and Performance

by

Murad Y. Abu-Farsakh, Ph.D., P.E.

Qiming Chen, Ph.D., PE

Louisiana Transportation Research Center

4101 Gourrier Avenue

Baton Rouge, LA 70808

LTRC Project No. 05-1GT

SIO No. 30000116

conducted for

Louisiana Department of Transportation and Development

Louisiana Transportation Research Center

The contents of this report reflect the views of the author/principal investigator who is responsible for the facts and the accuracy of the data presented herein. The contents do not necessarily reflect the views or policies of the Louisiana Department of Transportation and Development or the Louisiana Transportation Research Center. This report does not constitute a standard, specification, or regulation.

June 2014

ABSTRACT

The Louisiana Department of Transportation and Development (DOTD) has initiated a major effort to minimize the bridge end bump problem associated with differential settlement. As a result, a new design for the approach slab was proposed, which requires increasing the slab flexural rigidity (EI), and using reinforced soil foundation (RSF) to support the slab and traffic loads at the roadway pavement/approach slab joint (R/S joint). Reinforcing the soil underneath the strip footing will result in increasing the soil's bearing capacity and reducing the embankment settlement by redistributing the loads imposed by the slab and traffic over a wider area. Bayou Courtableau Bridge was selected as a demonstration project to evaluate, validate, and verify the new bridge approach slab design method proposed in a previous study. The east and west approach slabs at Bayou Courtableau Bridge are 40 ft. long by 40 ft. wide. The west approach slab was designed using the proposed new method with slab thickness of 16 in., while the east approach slab was designed using the traditional method with slab thickness of 12 in. The pavement end side of the approach slab was supported by a 4.0-ft. wide strip footing with the soil underneath it reinforced by six layers of geogrid placed at a vertical spacing of 12 in. The geosynthetic reinforced soil below the strip footing was designed according to the methodology proposed in previous study. The west approach slab was instrumented with pressure cells to measure the pressure distribution underneath the footing and contact pressure underneath the slabs. Strain gauges were used to measure strain distribution along geogrid reinforcement and sister-bar strain gauges to measure strains within the slab. The east approach slab was instrumented with pressure cells to measure the contact pressure underneath slab. Two static load tests were conducted on both the west and east approach slabs at two different times after construction. The performance of the approach slabs, including deformation and internal stresses of concrete slab, contact stresses between slab and embankment, stress distributions within reinforced soil foundation, and strain distributions along the geogrid, was monitored during the tests. The test results indicated that the west approach slab (with new design) lost most of its supports from the soil; while the east approach slab (with traditional design) kept losing its contacts from the soil starting from the bridge side towards the pavement side after about a year and half. The roughness profiles show better performance of the new approach slab system with much lower International Roughness Index (IRI) values. The year and a half monitoring program at Bayou Courtableau Bridge demonstrated much better performance of the new approach slab design system (west approach slab) compared to the traditional design. The magnitude and rate of embankment settlement at Bayou Courtableau Bridge site was also monitored (for the two embankment sides) during and after the construction, and the results were compared with the laboratory calculated settlements and the piezocone penetration test (PCPT)-based

settlement prediction methods. The results showed better predictions using PCPT methods as compared to laboratory results.

ACKNOWLEDGMENTS

This research project was funded by the DOTD (SIO No. 30000116) and the Louisiana Transportation Research Center (LTRC Project No. 05-1GT). The comments and suggestions of Mark Morvant, associate director of research; Zhongjie “Doc” Zhang, pavement and geotechnical administrator; and Gavin Gautreau, geotechnical engineering manager, of LTRC are gratefully acknowledged. The authors want to extend their thanks to Khalil Hanifa and Benjamin Comeaux for providing valuable assistance in this study. The help from the pavement research section is also greatly appreciated.

IMPLEMENTATION STATEMENT

In this research study, the Bayou Courtableau Bridge was selected as a demonstration project to evaluate, validate and verify the new approach slab design method proposed in a previous study aimed at minimizing the bridge end bump problem associated with the differential settlement [1]. For this purpose, the two embankment sides at Bayou Courtableau Bridge were instrumented and monitored over a period of one and a half years. The west approach slab was designed using the proposed new method and the east approach slab was designed using the traditional method. Static load tests were conducted and IRI measurements were performed at different times on both the east and west approach slabs for comparison. The results of this study clearly demonstrated the better performance of the new approach slab design method (west approach slab) over the traditional design method (east approach slab).

The researchers recommend that DOTD engineers start implementing the new design methodology for designing future approach slabs to mitigate the bridge end bump problem associated with the differential settlement (e.g., increasing the flexural rigidity (EI) of the approach slab and reinforcing the soil beneath the strip footing at the slab-pavement end). For the design of approach slab, DOTD engineers can follow the recommendations presented in the LTRC Final Report No. 403 [1]. The reinforced soil foundation used to support the slab and traffic loads can be designed using the analytical model proposed in the LTRC Final Report No. 424 [2].

The embankments' settlement at the Bayou Courtableau Bridge site was also monitored to verify the PCPT-based settlement prediction methods developed in a previous study [3]. The results showed that the PCPT settlement prediction methods can be implemented to estimate the magnitude and time rate of consolidation settlement of embankments.

TABLE OF CONTENTS

ABSTRACT.....	iii
ACKNOWLEDGMENTS	v
IMPLEMENTATION STATEMENT	vii
TABLE OF CONTENTS.....	ix
LIST OF TABLES.....	xi
LIST OF FIGURES	xiii
INTRODUCTION	1
OBJECTIVE	5
SCOPE	7
METHODOLOGY	9
Summary of Previous Research Findings.....	9
Approach Slab.....	9
Reinforced Soil Foundation	10
Bayou Courtableau Bridge Site	11
Design of Approach Slab System	14
Instrumentation Plan.....	16
Static Load Testing.....	16
Installation of Horizontal Inclinometer.....	20
Settlement Prediction.....	21
Constrained Modulus, M	22
Coefficient of Consolidation.....	23
DISCUSSION OF RESULTS.....	25
Design of Reinforced Soil Foundation	25
Contact Stresses	26
Internal Strain of the West Approach Slab	30
Stress Distribution within Reinforced Soil Foundation.....	31
Strain Distribution along the Geogrid.....	34
International Roughness Index (IRI) Measurement.....	35
Embankment Settlement.....	40
Field Measurement.....	40
Settlement Prediction	40
SUMMARY AND CONCLUSIONS	47
RECOMMENDATIONS	49
ACRONYMS, ABBREVIATIONS, AND SYMBOLS	51
REFERENCES	53

LIST OF TABLES

Table 1 Recommended slab thickness and major reinforcement [1]	9
Table 2 Recommended design parameters for reinforcement layout [2, 8]	10
Table 3 Properties of geogrid reinforcement	16
Table 4 Correlation equations of constrained modulus	22

LIST OF FIGURES

Figure 1 Illustration of approach slab and its interaction with soil.....	1
Figure 2 Failure mode of reinforced soil foundation: failure similar to footings on a two-layer soil system [2, 8].....	11
Figure 3 Profile of soil properties of east side subgrade.....	13
Figure 4 PCPT profiles and soil classification for Courtableau Bridge east site.....	13
Figure 5 Dissipation test for Courtableau Bridge west site	14
Figure 6 Standard and new approach slab design systems	15
Figure 7 Photos of instrumentation and data acquisition system.....	17
Figure 8 Cone truck locations during the static load tests	19
Figure 9 Large cone truck axle distribution and loads.....	20
Figure 10 Installation plan of horizontal inclinometers.....	21
Figure 11 Installation of horizontal inclinometer casing and return pipe.....	21
Figure 12 Contact stress between approach slab and embankment when the cone-truck was positioned at Location 3 (October 2009).....	27
Figure 13 Contact stress between approach slab and embankment when the cone-truck was positioned at Location 5 (October 2009).....	28
Figure 14 Contact stress between approach slab and embankment when the cone-truck was positioned at Location 3 (March 2011)	29
Figure 15 Contact stress between approach slab and embankment when the cone-truck was positioned at Location 5 (March 2011)	30
Figure 16 Internal strain distributions within the approach slab.....	32
Figure 17 Stress distributions within the reinforced soil foundation (October 2009)	33
Figure 18 Stress distributions within the reinforced soil foundation (March 2011).....	34
Figure 19 Strain distributions along the geogrid (October 2009).....	37
Figure 20 Strain distributions along the geogrid (March 2011)	37
Figure 21 Roughness profiles for three runs along the left wheelpath on the westbound lane	38
Figure 22 Average roughness profiles at eastbound and westbound lanes.....	38
Figure 23 Photos of R/S joints	39
Figure 24 Measured settlement profile	41
Figure 25 Comparison of constrained modulus and coefficient of consolidation	43
Figure 26 Comparison of Settlement Prediction.....	44
Figure 27 Rate of consolidation settlement	45

slabs are built (Figure 1). Based on previous studies, a 6 in. settlement will create a gap between approach slab and embankment soil (loss of support). When settlement occurs, the slab will bend in a concave manner that causes a sudden change in slope grade of the slab. Traffic loads will be redistributed to the ends of the slab. Due to the redistribution of loading, vertical faulting at the R/S joint and a sudden change in the slope of grade at the S/D joint may occur. Over time, the rideability of the bridge approach slabs will deteriorate.

The bump at the end of a bridge problem affects about 25 % of the bridges in the United States (approximately 150,000), and the amount of money spent every year on the repair of this problem nationwide is estimated to be at least \$100 million [4]. There are several ways to reduce the bump at the end of the bridge, such as pile supported embankment, lightweight embankment fill, etc. [5]. However, the cost of a particular solution may be prohibitive or exceed the life-cycle costs. The best current practices aim at optimizing the balance between proper design, proper construction, and acceptable maintenance while satisfying budget constraints and safety levels [4].

The Louisiana Department of Transportation and Development (DOTD) has launched a major effort to solve the bridge bump problem by changing the design of approach slabs where differential settlement is expected [1]. The objective is to find a feasible solution that makes the approach slabs strong enough to allow them to lose a portion or all of their contact supports without detrimental deflection. In this solution, the flexural rigidity (EI) of the approach slabs will be increased by increasing the slab thickness and reinforcement, and therefore some embankment settlement will be allowed without a decrease in ride quality [1]. As a result, the slab and traffic loads will be carried by the two ends of the slab (simply supported) rather than supported by distribution over the length of the slab. Accordingly, a footing will be needed to support the concentrated load at the R/S joint. To increase the bearing capacity of the embankment soil and to reduce the footing settlement due to concentration load, the soil underneath the footing need to be reinforced with geosynthetic reinforcement, such as geogrids.

Several research projects were initiated by DOTD and LTRC in response to this need, aiming at solving the bridge end bump problem [1, 2, 6]. Cai et al. investigated the effect of embankment settlements on the performance of the approach slab using a 3-D finite element analysis [1]. A correlation among the slab parameters, deflections of approach slabs, internal moments of the slab, and the differential settlement was established. A proper design of the approach slab was then provided to help mitigate the rideability problems of the slab in their study. Abu-Farsakh et al. identified the capability of geosynthetic reinforcement to increase

the soil's bearing capacity and to reduce the footing settlement [2]. Typical design parameters for reinforcement layout were recommended and a step-by-step procedure for RSF design was provided in their study. To validate the findings and the design recommendations developed in these research studies, and to update the design and construction guidelines of DOTD for bridge approach slabs to mitigate bridge end bump problem, the Bayou Courtableau Bridge was selected to demonstrate the new approach slab design system through instrumentation.

As mentioned earlier, the settlement of embankment contributes significantly to the development of bump problem at the end of the bridge. As a result, the accurate prediction of the embankment settlement becomes necessary for solving this issue. A reasonable estimate of the consolidation settlement of embankments on soft soil deposits requires better and more accurate evaluation of the consolidation parameters of the subsurface soils. In-situ tests, such as the piezocone penetration test (PCPT), can provide more accurate and reliable results than laboratory tests in evaluating the actual strength and consolidation properties of the soil under in-situ stress and drainage conditions. The PCPT has gained wide popularity and acceptance for subsurface investigation and soil characterization. The piezocone penetrometer is capable of measuring the profile of cone tip resistance, q_c , sleeve friction, f_s , and porewater pressure, u , at different locations. These measurements can be effectively used for soil identification and evaluation of different soil properties such as the consolidation characteristics of soils.

Continuous efforts have been made in Louisiana to improve the accuracy of prediction of the embankment settlement using PCPT measurements [3, 7]. New empirical calibration equations of constrained modulus and coefficient of consolidation were proposed in these studies. The research team at the Louisiana Transportation Research Center (LTRC) has selected the Courtableau Bridge site to verify the proposed PCPT based method for prediction of embankment settlement. In this report, the subsurface soil properties were evaluated using both laboratory testing and in-situ PCPT penetration and dissipation tests. Horizontal inclinometers were installed on both embankment sides of the bridge; and readings were taken at specified time intervals during and after construction. Predicted settlement by both the laboratory and PCPT methods were compared with the measured settlement to evaluate the performance of each method.

OBJECTIVE

The main objective of this research project is to perform field testing and monitoring on instrumented concrete approach slabs to validate the findings and design recommendations developed in the previous research projects and to update the design and construction guidelines of DOTD for bridge approach slabs to mitigate the bridge end “bump” problem. The validity of the proposed PCPT based method for prediction of embankment settlement was also evaluated in this study.

SCOPE

To achieve the objectives of this research study, the Bayou Courtableau Bridge was selected to demonstrate the new approach slab design system [1 , 2]. The west approach slab of the bridge was designed using the proposed new method and the east approach slab was designed using the traditional method. The west approach slab was instrumented with pressure cells to measure the contact stress below the slab and stress distribution underneath the strip footing and within the reinforced soil foundation. Strain gauges were used to measure strain distribution along geogrids, and sister-bar strain gauges to measure the internal stresses within the concrete slab. The east approach slab was instrumented with pressure cells to measure the contact stress below slab and stress distribution underneath the “sleeper” strip footing. The two embankment sides were instrumented and monitored over a period of one and a half years. Static load tests were conducted and IRI measurements were performed at different times to evaluate the performance of the two approach slabs. The field performance measurements, including deformation and internal stresses of the concrete slabs, contact stresses between slab and embankment, stress distributions within the reinforced soil foundation, and strain distributions along the geogrids, were monitored and will be presented in this report. Horizontal inclinometers were also installed on both embankment sides of the bridge to monitor the embankments’ settlements at specified time intervals during and after construction. The predicted settlements by both the laboratory and PCPT estimation methods were compared with the field measurements.

METHODOLOGY

As discussed earlier, the main objective of this research study was to perform field tests on concrete approach slabs to validate the findings and design recommendations developed in the previous research projects [1, 2]. Background information on two previous projects was introduced first. Then the Bayou Courtableau Bridge was selected to demonstrate the new approach slab design system. The field performance, including deformation and internal stresses of the concrete slabs, contact stresses between slab and embankment, stress distributions within reinforced soil foundation, and strain distributions along the geogrid, was monitored. The embankment settlement was measured at specified time intervals using horizontal inclinometers. The predicted settlement using laboratory data, the Sanglerat method, and the proposed method was compared with field measurements.

Summary of Previous Research Findings

Approach Slab

A 3-D finite element analysis was conducted to examine the interaction between the approach slab and the embankment soil, and, consequently, the separation of the slab and soil in a previous project (03-4GT) [1]. The results showed that with the increase in slab thickness and reinforcement (stiffer), the slab deformation can be well controlled. Therefore, considering different levels of embankment settlements, an engineer can either use a thicker approach slab and/or more reinforcement (stiffer) to allow partial or full separation between the embankment and the approach slab. The recommended approach slab thickness and major reinforcement (bottom layer in the span direction) for flat approach slabs with a span length of 40 ft. are presented in Table 1.

Table 1
Recommended slab thickness and major reinforcement [1]

Differential settlement (in)	Recommended		Current Design
	18 in. slab	24 in. slab	12 in. slab
0.0	#7@16"	#6@11"	#6@6"
0.6	#8@6.0"	#8@6.5"	
1.2	#9@5.5"	#10@8.0"	
2.4	#10@6.0"	#10@8.5"	
3.6~7.2	#10@5.5"	#10@8.5"	

Reinforced Soil Foundation

As mentioned earlier, the new approach slab design allows partial or full separation between the embankment and the slab. As a result, the slab dead load and traffic load are transferred to the abutment and the sleeper slab; and the local soil pressures beneath the sleeper slab increase, thereby increasing the faulting deflection (δ_D in Figure 1). Geosynthetics can be used to reinforce the soil beneath the sleeper slab, thereby increasing the soil's bearing capacity, helping redistribute the load to a wider area, hence reducing the sleeper slab's settlement. Extensive experimental studies, including small-scale laboratory model tests and large-scale field tests, were conducted on geosynthetic reinforced embankment soils by the authors in a previous project (04-2GT) [2]. The influences of different variables and parameters contributing to the improved performance of reinforced soil foundation (RSF) were examined in these tests. This includes the depth of the first reinforcement layer (u), the total depth of reinforcement (d), the vertical spacing between reinforcement layers (h), the length of reinforcement (l) and the tensile modulus (J), and type of reinforcement. The recommended parameters for layout of the reinforcement are shown in Table 2.

Table 2
Recommended design parameters for reinforcement layout [2, 8]

Parameter	Typical value	Recommended
u/B	0.2 ~ 0.5	1/3
h/B	0.2 ~ 0.5	1/3
d/B	1.3 ~ 1.7	1.5
l/B	4 ~ 6	5

The reinforced soil foundation in this study is considered to be a two layer system, i.e., under the ultimate load, a punching shear failure will occur in the reinforced zone followed by a general shear failure in the underlying soil layer as shown in Figure 2 [2, 8].

This type of failure mode was first suggested by Meyerhof and Hanna for stronger soil overlying weaker soil [9]. To include the benefits of geosynthetic reinforcement, the authors modified Meyerhof and Hanna's solution through attributing the geosynthetic reinforcement effect to provide additional confining stress to the punching wedge aa'b'b [2, 8].

$$q_{u(R)} = q_b + \frac{2c_a d}{B} + \gamma_t d^2 \left(1 + \frac{2D_f}{d} \right) \frac{K_s \tan \phi_t}{B} + \frac{2 \sum_{i=1}^N T_i \tan \delta}{B} - \gamma_t d \quad (1)$$

$$q_b = c_b N_c + q N_q + 0.5 \gamma_b B N_\gamma \quad (2)$$

where, $q_{u(R)u(R)}$ is the ultimate bearing capacity of reinforced soil foundation (here, reinforced unpaved section); q_b is the ultimate bearing capacity of the underlying unreinforced soil; c_a is the unit adhesion along the sides of the punching wedge $aa'b'b'$; d is the thickness of the reinforced zone; B is the width of the footing; γ is the unit weight of soil in the reinforced zone; D_f D_f is the embedment depth of the footing; K_s K_s is the punching shear coefficient for the reinforced zone, which depends on the friction angle of soil in the reinforced zone and the ultimate bearing capacity of soil in both the reinforced zone and the underlying unreinforced zone; ϕ_i is the friction angle of soil in the reinforced zone; N is the number of reinforcement layers; T_i is the tensile force in the i^{th} layer of reinforcement; δ is the mobilized friction angle along the sides of the punching wedge $aa'b'b'$; N_c , N_q , N_γ are the bearing capacity factors, which are dependent on the friction angle of soil in the underlying unreinforced zone ϕ_b ; c_b is the cohesion of soil in the underlying unreinforced zone; q is the surcharge load = $\gamma(D_f+d)$; and γ_b is the unit weight of soil in the underlying unreinforced zone.

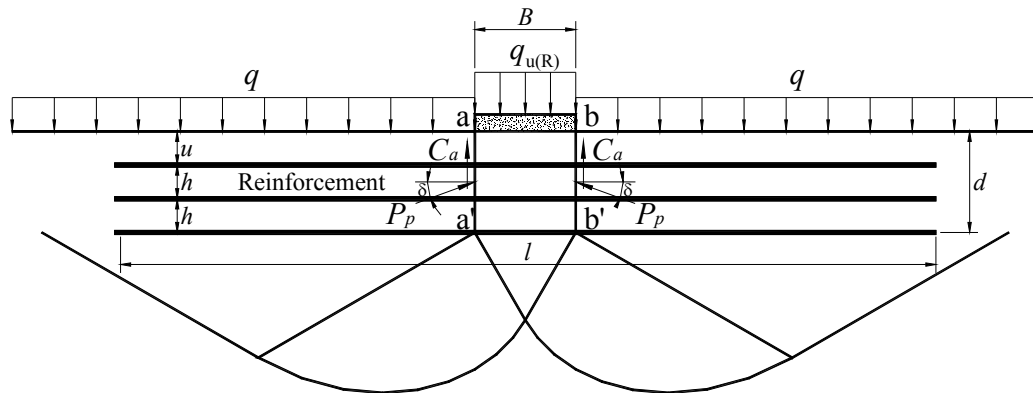


Figure 2

Failure mode of reinforced soil foundation: failure similar to footings on a two-layer soil system [2, 8]

Bayou Courtableau Bridge Site

The Bayou Courtableau Bridge, as part of Louisiana Highway 103 in St. Landry Parish, is located 2 miles east of I-49 highway. Replacement of the old bridge, which was built in 1930, was required because of its low sufficiency rating (a rating of 10 or less), according to DOTD. The sufficiency rating is a numerical value ranging from 0 to 100, with 55 percentage points applied to the structural adequacy, 30 percent points applied to the functional adequacy and serviceability, and 15 percent points applied to the essential for

public use. A sufficiency rating of less than 50 qualifies a bridge for replacement, while a sufficiency rating of less than 80 qualifies a bridge for rehabilitation [10].

A comprehensive field and laboratory testing program was conducted to investigate the soil properties of the bridge site, which included moisture content, density, Atterberg limits, particle size analysis, 1-D consolidation tests, UU tests, k_0 -CU tests, and piezocone penetration and dissipation tests. The 1-D consolidation test results along with soil strata from soil boring logs are presented in Figure 3. The first column of the plots shows the soil strata obtained from the boring log of the bridge site; the second column presents the moisture content (m.c.), liquid limit (L.L.), and plastic limit (P.L.) results of Shelby tube samples obtained from the site; the undrained shear strength (S_u) from UU test is shown in the next column; the constrained modulus (M) and coefficient of consolidation (c_v) at the in-situ stress level determined from the laboratory 1-D consolidation tests are shown in the following two columns, respectively; the last column plots the profile of overconsolidation ratio (OCR). These parameters were used in the calculation of embankment settlement in the later section. One CPT test was conducted on each embankment site of the bridge to profile the subsurface soils for settlement estimation. The profiles of CPT test results (q_t , f_s , and R_f) and the corresponding CPT soil classification, using the Zhang and Tumay CPT classification method, are presented in Figure 4 [11]. As shown by the CPT soil classification, the subsurface soil mainly consists of clayey silt in the upper 60 ft. (18.3 m) below ground surface. Compared to the west embankment site, the east site is a little sandier. Several dissipation tests were conducted at each side of the bridge as shown in Figure 5 to obtain the consolidation parameters used for settlement estimation. The depths for the PCPT dissipation tests at the west side embankment are 1.96, 2.64, 3.83, 7.60, 9.55, 13.88, 16.15, and 18.15 m below the old pavement surface.

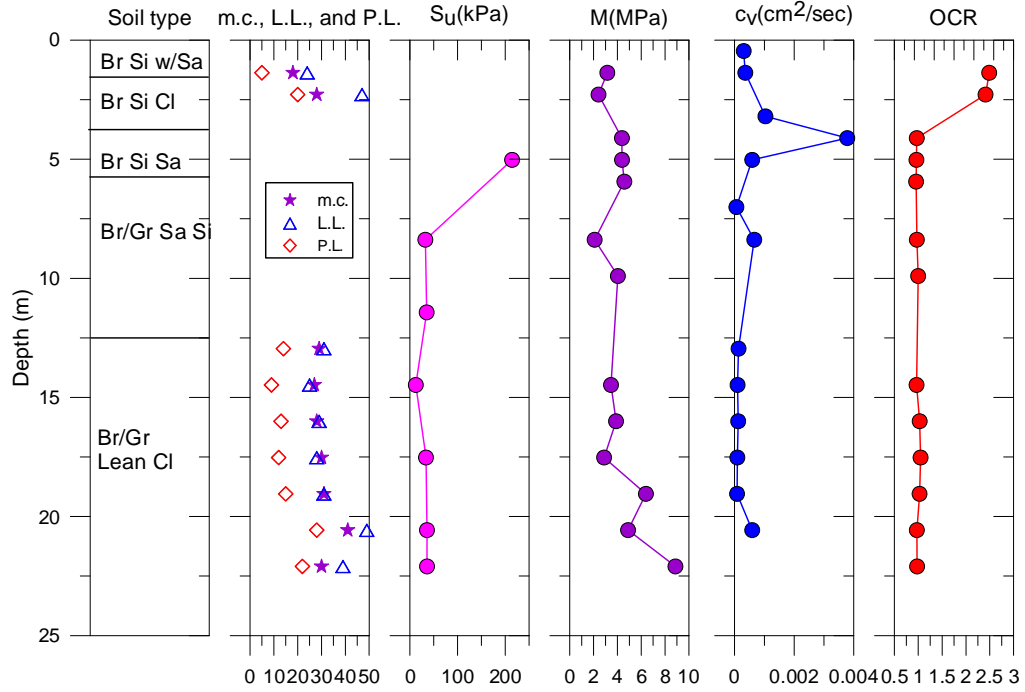


Figure 3
Profile of soil properties of east side subgrade

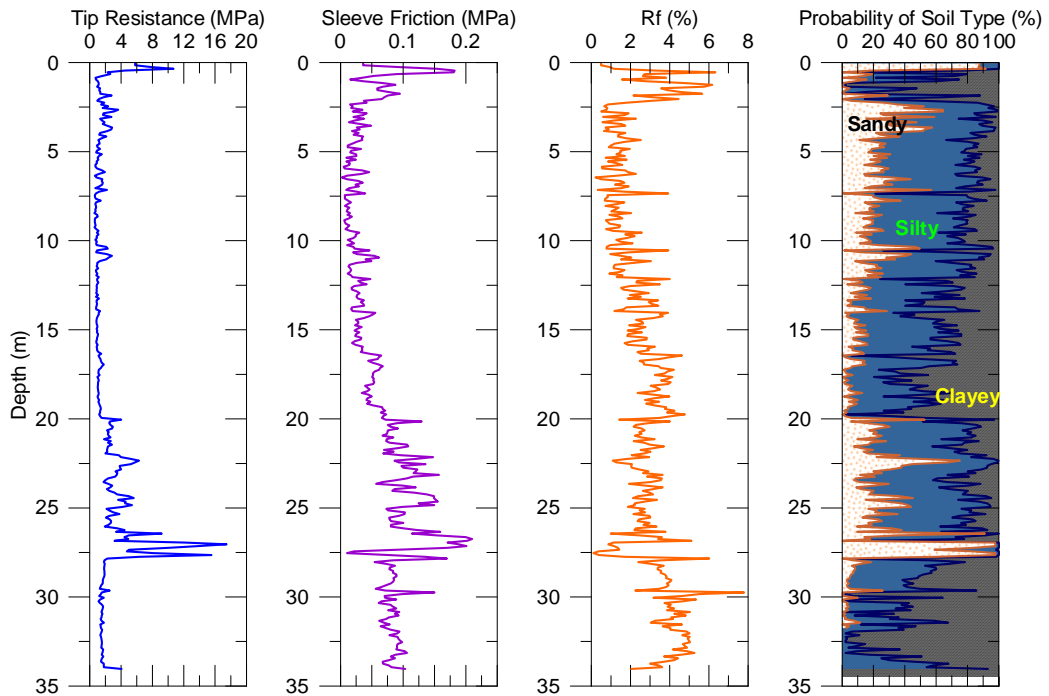


Figure 4
PCPT profiles and soil classification for Courtableau Bridge east site

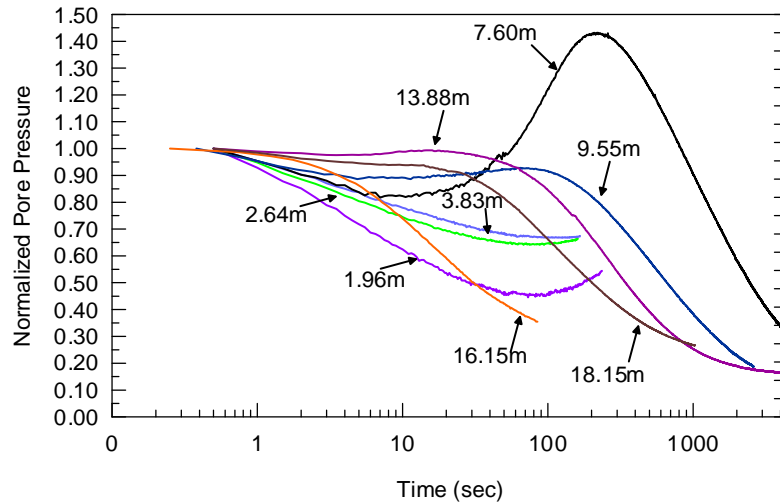


Figure 5
Dissipation test for Courtableau Bridge west Site

Design of Approach Slab System

The east approach slab of the bridge was designed according to standard (traditional) DOTD's Bridge Design Specifications for comparison. The thickness of the slab is 12 in. The No. 6 steel bars were placed at 6 in. spacing at the bottom of slab, while No.4 steel bars were installed at the top of slab at a spacing of 12 in. The design of the west approach slab of the bridge was changed to follow the new proposed approach slab design system [1]. The rigidity of the west approach slab was increased by increasing the thickness from standard 12 in. to 16 in. The bottom slab steel bars was increased from No. 6 to No. 10, while the other reinforcement configurations remained the same as the east approach slab. A 4-ft. wide strip footing (B=4 ft.) was placed at the roadway pavement/approach slab joint to support the slab dead load and traffic loads. The soil underneath the footing was reinforced with six layers of BX1500 geogrid placed at a spacing of 12 in., as described in Figure 6. The physical and mechanical properties of the geogrid, as provided by the manufacturer, are summarized in Table 3. The embankment fill is a silty clay, having a liquid limit of 41 and a plastic index of 23. This soil contains 53% silt, 46% clay, and 1% sand. The maximum dry density of the soil is 99.4 lb/ft³ with an optimum moisture content of 15.8% as determined by Standard Proctor test. This silty clay soil was classified as CL according to the Unified Soil Classification System (USCS), and A-7-6(24) according to the AASHTO classification system.

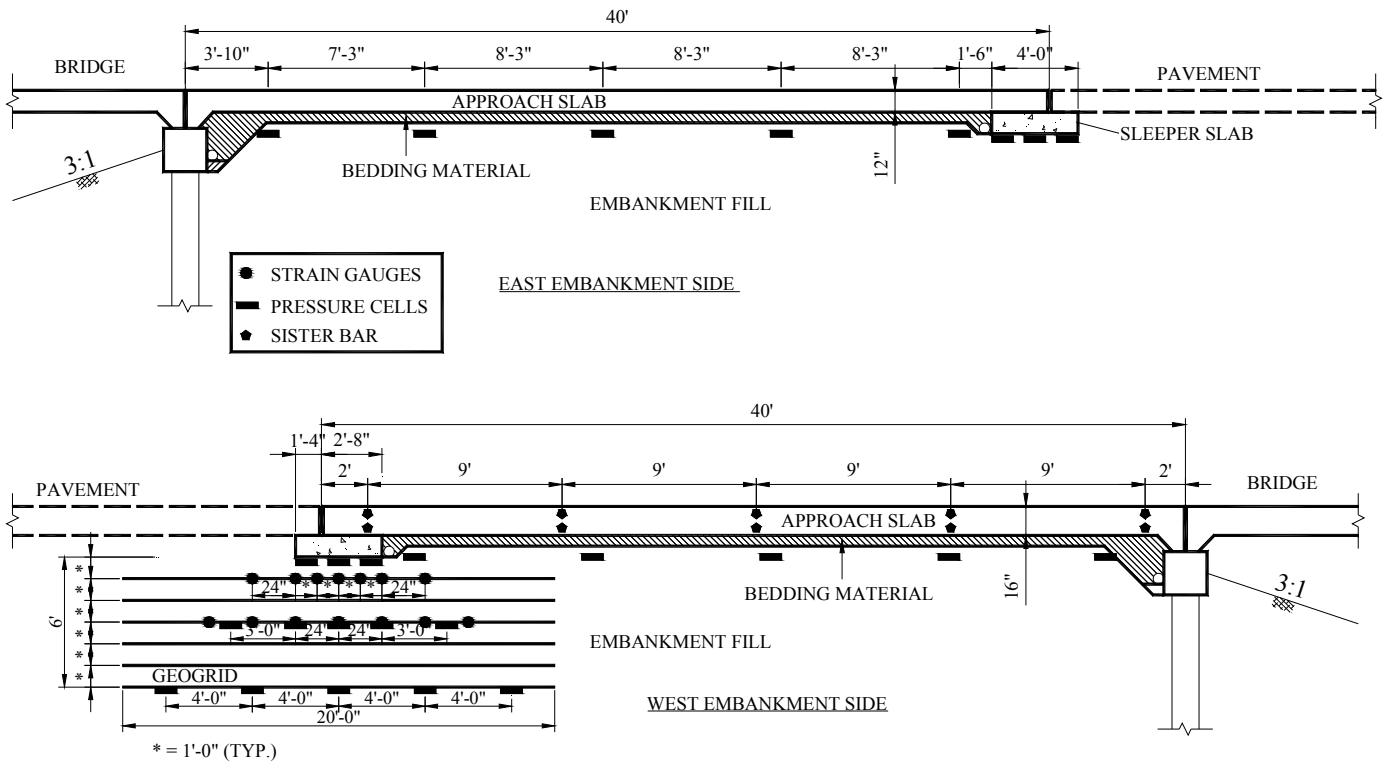


Figure 6
Standard and new approach slab design systems

Table 3
Properties of geogrid reinforcement

Reinforcement	Polymer Type	T ^a , lb/ft		J ^b , lb/ft		Aperture Size, in
		MD ^c	CD ^d	MD ^c	CD ^d	
Tensar BX1500 geogrid	Polypropylene	580	690	29000	34500	1.0×1.2

^aTensile Strength (at 2% strain), ^b Tensile Modulus (at 2% strain), ^cMachine Direction, ^dCross machine direction

Instrumentation Plan

To monitor the performance of the new approach slab system, an instrumentation plan, which included electrical resistance strain gages (Vishay Micro-Measurements EP-08-250BG-120), pressure cells (Geokon Model 4800), and “sister bar” strain gages (Geokon Model 4911) (Figure 7), was developed and deployed. Five pressure cells were installed underneath the approach slabs of each side to investigate the contact stress between the slab and embankment (Figure 6). To investigate the stress distribution within reinforced soil foundation, three pressure cells were installed below the strip footings of each side; ten pressure cells were installed within the reinforced zone under the strip footing of the west approach slab (Figure 6). To investigate the strain distribution along the geogrid reinforcement, two layers of geogrids were instrumented with the strain gages with locations at 1 ft. below and 3 ft. below the strip footing as shown in Figure 6. To evaluate the internal stress of the approach slab, fifteen pairs of “sister bar” strain gages were installed within the west approach slab (Figure 7).

Static Load Testing

Two static load tests were conducted on both west and east approach slabs at Bayou Courtableau Bridge to evaluate their performance. The first one was conducted right before the bridge opened to traffic (October, 2009). The second was conducted one and half years later (March, 2011). Dead loads were placed on the slab by positioning the 20-ton large cone truck at strategic locations, as shown in Figure 8. The axle distribution and loads per axle of the large cone truck are described in Figure 9.

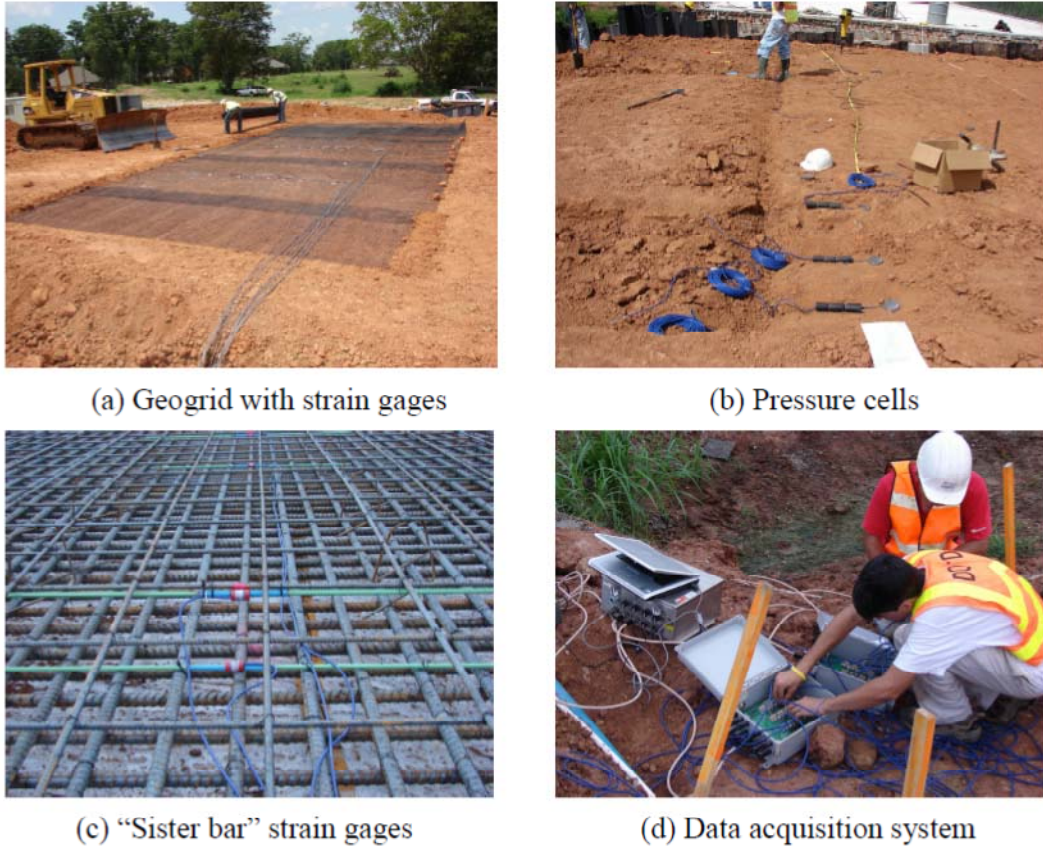
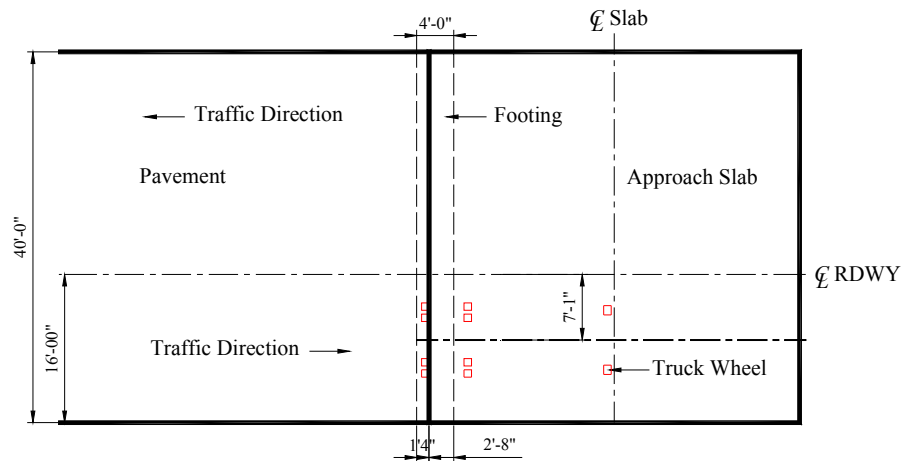
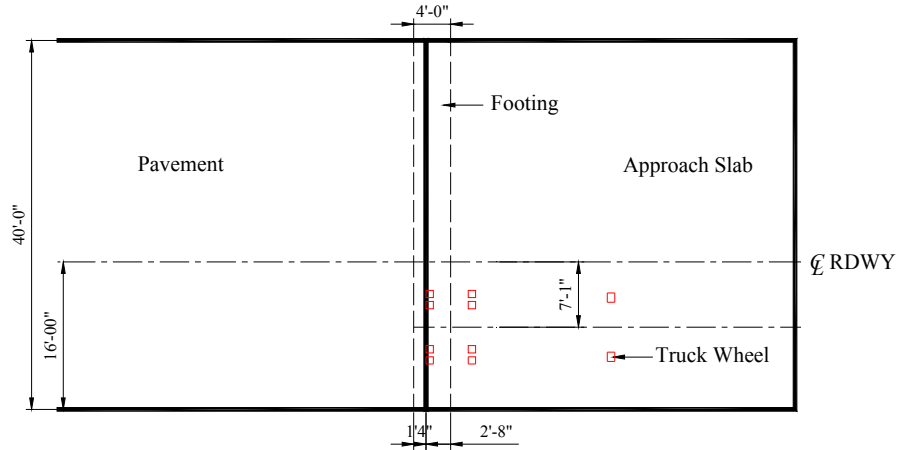


Figure 7
Photos of instrumentation and data acquisition system

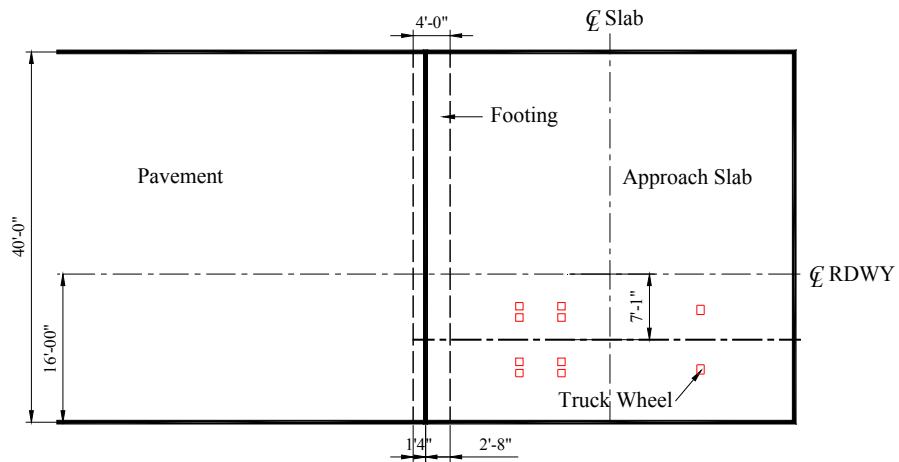


(a) Location 1

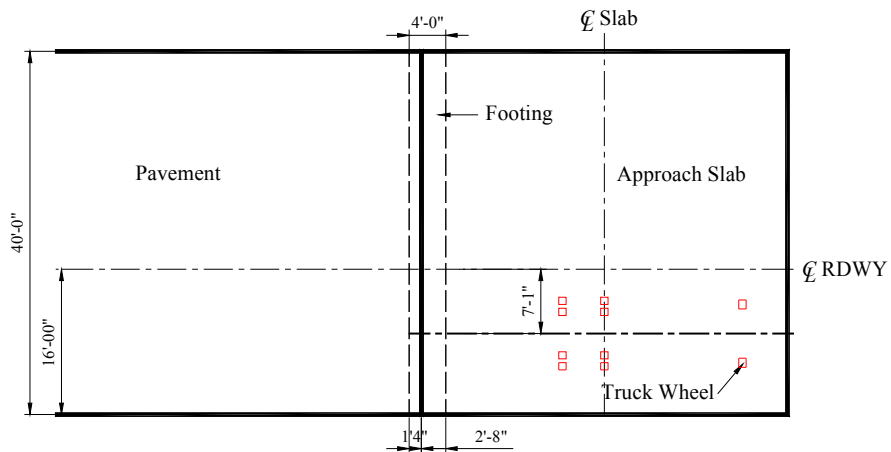
Figure 8 (continued)



(b) Location 2

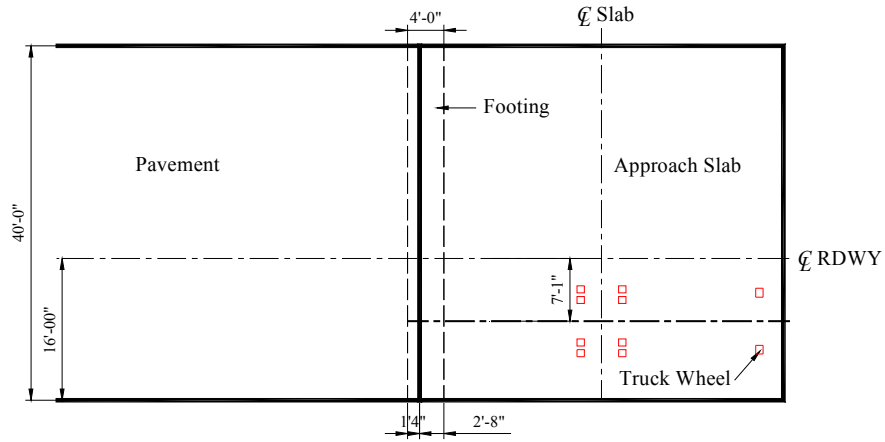


(c) Location 3

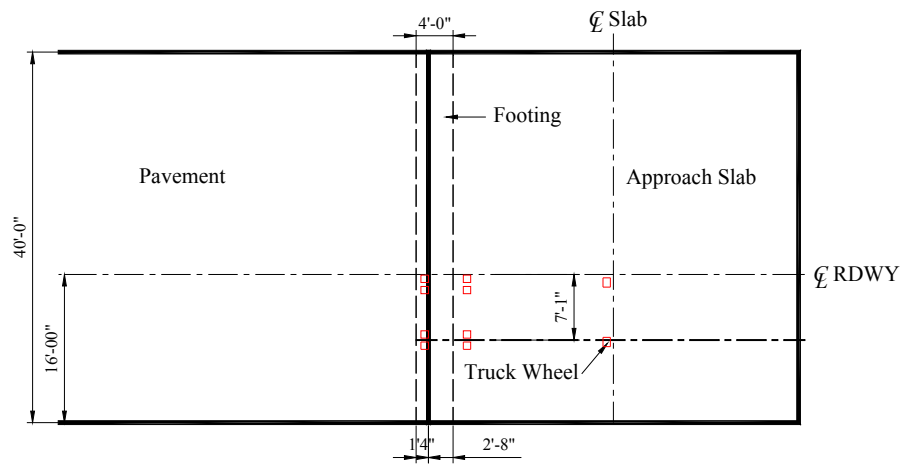


(d) Location 4

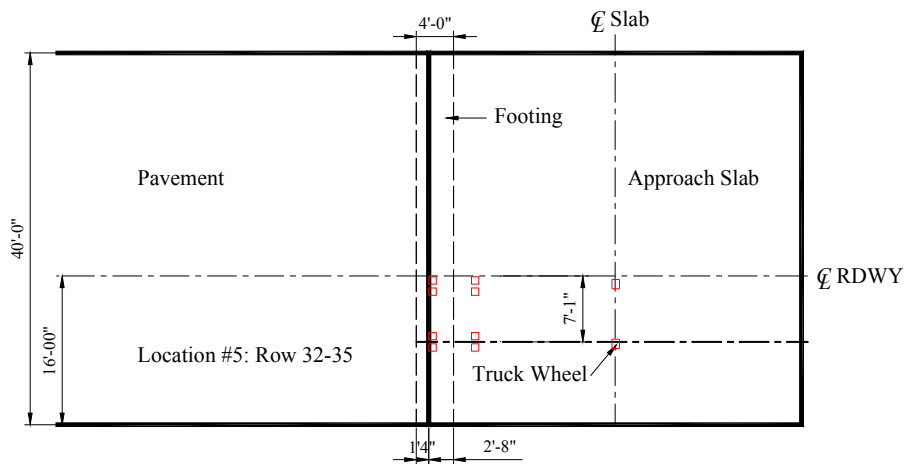
Figure 8 (continued)



(e) Location 5



(f) Location 6



(d) Location 6

Figure 8
Cone truck locations during the static load tests

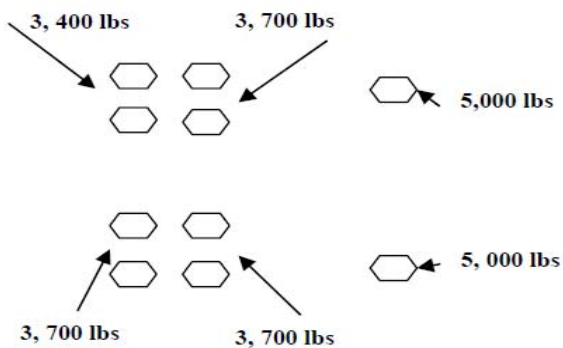


Figure 9
Large cone truck axle distribution and loads

Installation of Horizontal Inclinometer

The newly constructed east embankment has a height of 8 ft. above the existing pavement and a width of 120 ft.; the newly constructed west embankment has a height of 6 ft. above the existing pavement and a width of 110 ft. One horizontal inclinometer was installed at each embankment side underneath the middle of the approach slab to monitor the profile of consolidation settlement of subsurface soil along the embankment cross section. The installation plan of the inclinometers is shown in Figure 10. A 2-ft. wide and 2-ft. deep trench, as shown in Figure 11, was dug after the completion of the first lift of embankment fill. The return pipe with a diameter of 3.34 in. (85 mm) and casing were also aligned on the bottom of the trench. The trench was then backfilled and manually compacted with a hand compactor. In this study, a digital horizontal inclinometer system manufactured by RST instruments Ltd. was used, which consists of inclinometer casing, a horizontal probe, control cable, and a readout unit. Each end of the inclinometer casing extended about 10 ft. beyond the embankment and was fastened to two wooden posts inserted deep into the natural ground to provide stable reference points for future survey. A first survey was conducted immediately after the trench was compacted to obtain the baseline survey in addition to check the function of the casing. The inclinometer probe was pulled through the casing twice with the probe in forward and backward position at a 2-ft. interval, i.e. the length of probe. The two readings can eliminate possible errors of the instrument and provide accurate measurement of settlement profile. The inclinometer readings were taken at specified time intervals until 6 months after the completion of the construction.

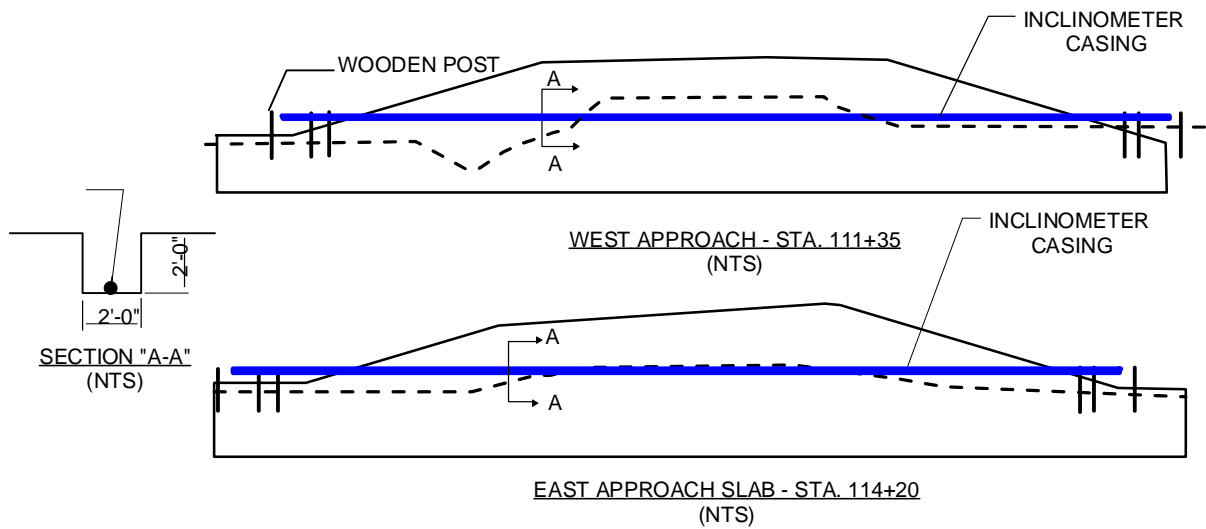


Figure 10
Installation plan of horizontal inclinometers



Figure 11
Installation of horizontal inclinometer casing and return pipe

Settlement Prediction

The magnitude of total consolidation settlement (S_c) of fine-grained soil can be estimated utilizing the constrained modulus (M) predicted from the PCPT measured data using the following equation:

$$S_c = \sum H_i \frac{\Delta\sigma_i}{M_{avi}} \quad (3)$$

where, H_i is the thickness of the soil layer i , $\Delta\sigma_i$ is the induced stress in the mid of layer i , and M_{avi} is the average constrained modulus of soil layer i for a stress range from initial in-situ vertical stress to the final vertical stress after the completion of embankment fills [12, 13].

Constrained Modulus, M

Several correlations have been proposed to estimate the constrained modulus from either the cone tip resistance (q_c) or the corrected cone tip resistance (q_t) [3]. The general relationship for M can be expressed as follows:

$$M = \alpha \cdot q_c \quad \text{or} \quad M = \alpha \cdot q_t \quad (4)$$

$$q_t = q_c + (1 - \alpha)u_2 \quad (5)$$

where, α is A_n/A_c ; A_n is the cross-sectional area of the load cell and A_c is the projected area of the cone. Some of the popular correlation equations of constrained modulus are summarized in Table 4. Sanglerat presented a comprehensive array of α values for different soil types with different cone tip resistance values [14]. Senneset presented a correlation based on corrected tip resistance (q_t) for silty soils [12]. Senneset et al. presented a correlation based the tip resistance corrected by in situ soil vertical stress (σ_{vo}) for clayey soils [13]. Abu-Farsakh and Abu-Farsakh et al. evaluated the aforementioned correlation equations based on test data on Louisiana soils and proposed two correlation equations as shown in Table 4 [3, 7].

Table 4
Correlation equations of constrained modulus

Model	Equation
Sanglerat [14]	$\alpha \cdot q_c$, table of α provided in the reference
Senneset et al. [12]	$2q_t$ for $q_t \leq 2.5$ MPa $4q_t$ for $2.5 < q_t < 5$ MPa Silty soil
Senneset et al. [13]	$\alpha_p \cdot q_n = \alpha_p \cdot (q_t - \sigma_{vo})$ Pre-consolidation clay $\alpha_n \cdot q_n = \alpha_n \cdot (q_t - \sigma_{vo})$ Normal consolidation clay
Kulhawy and Mayne [15]	$8.25(q_t - \sigma_{vo})$
Abu-Farsakh [3] and Abu-Farsakh et al. [7]	$3.15 q_t$ $3.58 (q_t - \sigma_{vo})$

Coefficient of Consolidation

The piezocone dissipation tests can provide the estimation of in-situ coefficient of consolidation of subsurface soils. Dissipation test consists of stopping the cone penetration at a certain depth and recording the dissipation of excess pore pressure (Δu) with time. The excess pore pressure is defined as the difference between the penetration pore pressure (u) and the static equilibrium pore pressure (u_o).

In this study, the Teh and Houlsby method was used to estimate the horizontal coefficient of consolidation of the soil near the cone tip as shown in equation (5) [16].

$$c_h(\text{piezo}) = (T_{50}^* r_o^2 \sqrt{I_r}) / t_{50} \quad (5)$$

where, T_{50}^* is a modified time factor at 50% dissipation ($T_{50}^* = 0.118$ for the u_1 piezocone and 0.245 for the u_2 piezocone), $I_r = G/s_u$ is the rigidity index, G is the shear modulus, and s_u is the undrained shear strength. The shear modulus at 50% of yield stress (G_{50}) is usually used, which represents an average value of stress levels. Unconsolidated undrained (UU) tests and k_o -CU tests on retrieved soil samples were performed to determine the unstrained shear strength s_u and the shear modulus G at 50% yield stress, respectively. The determined s_u and G were used to determine the rigidity index I_r .

Since the dissipation of pore pressure occurs during the recompression range rather than in the normal consolidation range, Levadoux and Baligh suggested that the predicted $c_h(\text{piezo}) = c_h(\text{overconsolidated})$ and proposed the following relation to transfer $c_h(\text{piezo})$ to normally consolidated condition, $c_h(\text{NC})$ [17]:

$$c_{h(\text{NC})} = \frac{RR}{CR} c_h(\text{piezo}) \quad (6a)$$

where,

$$RR = \frac{c_r}{1 + e_o} \quad \text{and} \quad CR = \frac{c_c}{1 + e_o} \quad (6b)$$

where, RR and CR are the modified compression index and the modified recompression index, respectively; c_r is the swelling index; c_c is the compression index; and e_o is the initial void ratio of the soil. The vertical coefficient of consolidation (c_v) can then be calculated using the ratio of vertical to horizontal coefficients of hydraulic conductivity (k_v/k_h) using the following expression suggested by Levadoux and Baligh [17]:

$$c_{v(\text{NC})} = \frac{k_v}{k_h} c_{h(\text{NC})} \quad (7)$$

DISCUSSION OF RESULTS

Design of Reinforced Soil Foundation

The physical properties of the embankment soil have been determined from laboratory tests as, $c = 3.63$ psi (25 kPa), $\phi_t = 24^\circ$. The punching shear coefficient, K_s , the adhesion, c_a , and the mobilized friction angle, δ , can be determined by the charts provided by Meyerhof and Hanna as 4, 3.63 psi, and 24° , respectively [9]. By following Table 2, the geogrid layout parameters selected in this study are: $u/B = h/B = 0.25$, $d/B = 1.5$, $l/B = 5$. By following the recommendations presented in the Final Report No. 403 [2], the tensile strain can be estimated as 1.5% and 0.5% for top and bottom geogrid layers, respectively. The corresponding strains for geogrids located between the top and bottom layers were approximately linearly interpolated. The following are the estimated strains in the geogrid reinforcement layers at different levels:

$$\varepsilon_1 = 1.5\%, \varepsilon_2 = 1.3\%, \varepsilon_3 = 1.1\%, \varepsilon_4 = 0.9\%, \varepsilon_5 = 0.7\%, \text{ and } \varepsilon_6 = 0.5\%$$

Design Steps:

Step 1: The tensile force developed in the reinforcement at different levels was calculated:

$$T_1 = 435 \text{ lb/ft}, T_2 = 377 \text{ lb/ft}, T_3 = 319 \text{ lb/ft}, T_4 = 261 \text{ lb/ft}, T_5 = 203 \text{ lb/ft}, \text{ and } T_6 = 145 \text{ lb/ft}$$

Step 2: Calculate the ultimate bearing capacity of the unreinforced embankment soil:

$$N_q = 9.603, N_c = 19.324, N_\gamma = 9.442, d = 6 \text{ ft}, \text{ and } D_f = 0 \text{ ft.}$$

$$q_b = cN_c + \gamma(d + D_f)N_q + 0.5\gamma BN_\gamma = 85 \text{ psi}$$

Step 3: Calculate the ultimate bearing capacity of the reinforced embankment soil:

$$K_s = 4, c_a = 3.63 \text{ psi}, \delta = 24^\circ$$

$$q_{u(R)} = q_b + \frac{2c_a d}{B} + \gamma_t d^2 \left(1 + \frac{2D_f}{d} \right) \frac{K_s \tan \phi_t}{B} - \gamma_t d + \frac{2 \sum_{i=1}^N T_i \tan \delta}{B} = 153 \text{ psi}$$

So the ultimate bearing capacity of the embankment soil is increased by 80% with the inclusion of six layers of geogrid reinforcement.

The dead and live loads acting on the strip footing are estimated as 5.4 kips/ft and 5 kips/ft, respectively. These loads induce a footing pressure of 18 psi, which is significantly below the ultimate bearing capacity of both unreinforced and reinforced embankments soil. However,

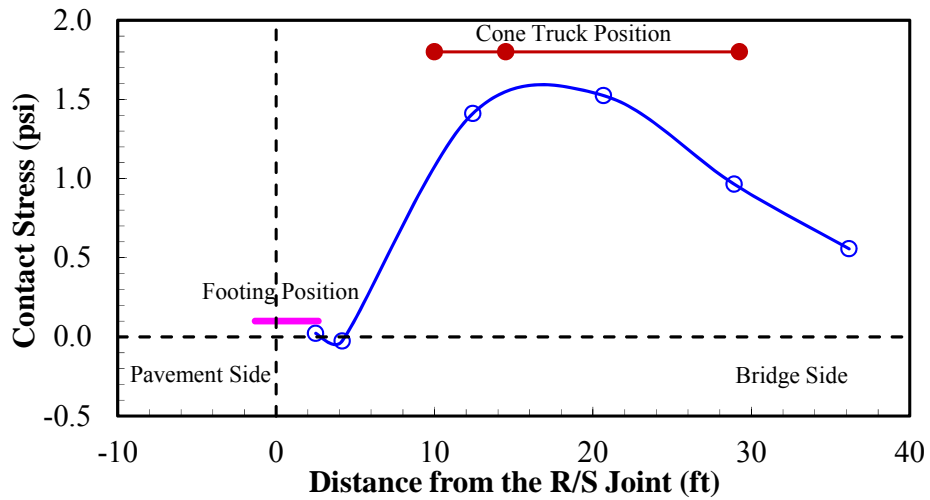
the control factor for the performance of approach slab would be the settlement of the strip footing.

Contact Stresses

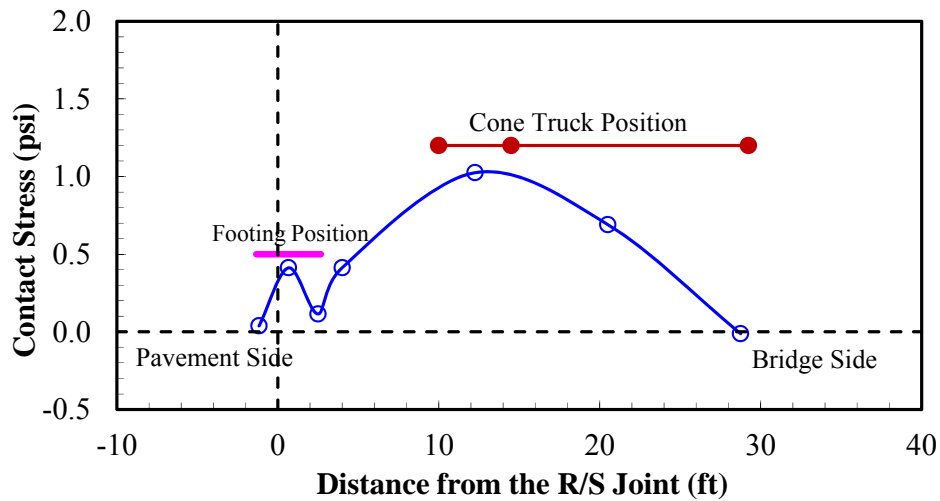
Figure 12a and 12b present the contact stresses measured between the slab and the embankment soil for each embankment side during the first static load test (October, 2009) when the 20-ton cone truck was positioned at the center of the slab, i.e., Location 3 as shown in Figure 8c. Figure 13a and 13b shows the contact stresses measured when the 20-ton cone truck was positioned at Location 5 as shown in Figure 8e. Two pressure cells below the strip footings of west side were out of order during the static load test. As can be seen from Figure 12a, all pressure cells underneath the west concrete approach slab (except for the one close to the R/S joint) registered significant pressures. This observation suggests that the west approach slab maintained its contacts and supports from the soil when the bridge was opened to the traffic. The same observation can be found in Figure 13a. The negligible registered pressures of the pressure cell close to the R/S joint may be due to the edge lift (curling) induced by the center loading. On the other hand, Figure 12b shows that for the east approach slab, the pressure cell close to the B/S joint (i.e., the pressure cell underneath the front axle of the cone truck for the truck position shown in the figure) registered negligible pressure. This observation may indicate that the east approach slab started partially losing its contacts and supports from the embankment soil before the bridge was opened to the traffic. The same observation can be found in Figure 13b. Interestingly, the pressure cells below the strip footings of the east side registered negligible pressures when the cone truck was positioned at Location 5. This may be due to the edge lift (curling) induced by the cone truck loading.

Figure 14a and 14b present the contact stresses measured between the slab and embankment of each side during the second static load test when the 20-ton cone truck was positioned at Location 3, as shown in Figure 8c (March, 2011). The contact stresses measured when the 20-ton cone truck was positioned at Location 5, as shown in Figure 8e, were presented in Figure 15a and 15b. It should be pointed out here that two pressure cells below the strip footings of west side and one pressure cell next to the B/S joint under the east approach slab were out of order during the static load test. As compared to the first static load test, the pressure cells under the west approach slab registered significantly lower pressures during the second static load test (Figure 14a). This observation suggests that the west approach slab already lost most of its contacts and supports from the soil by March 2011, i.e., the benefit of RSF is being mobilized. The same observation can be found in Figure 15a. Meanwhile, for the east approach slab, Figure 14b shows that the lower pressures registered during the

second load test only occurred in the pressure cells close to the B/S joint. This indicates that the east approach slab was gradually losing its contacts and supports from the bridge side towards the pavement side. The same observation can be found in Figure 15b. Similar to the first static load test, the pressure cells below the strip footings of east side registered negligible pressures when the cone truck was positioned at Location 5.

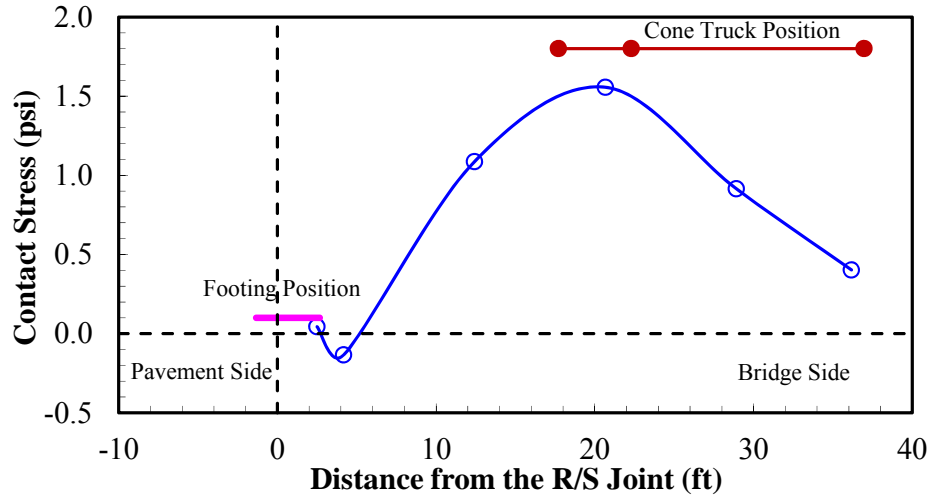


(a) West approach slab

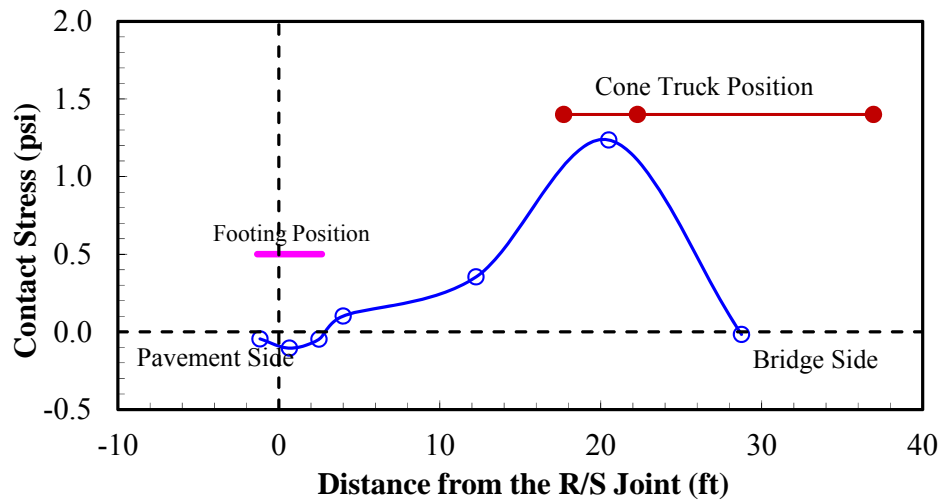


(b) East approach slab

Figure 12
Contact stress between approach slab and embankment when the cone-truck was positioned at Location 3 (October 2009)

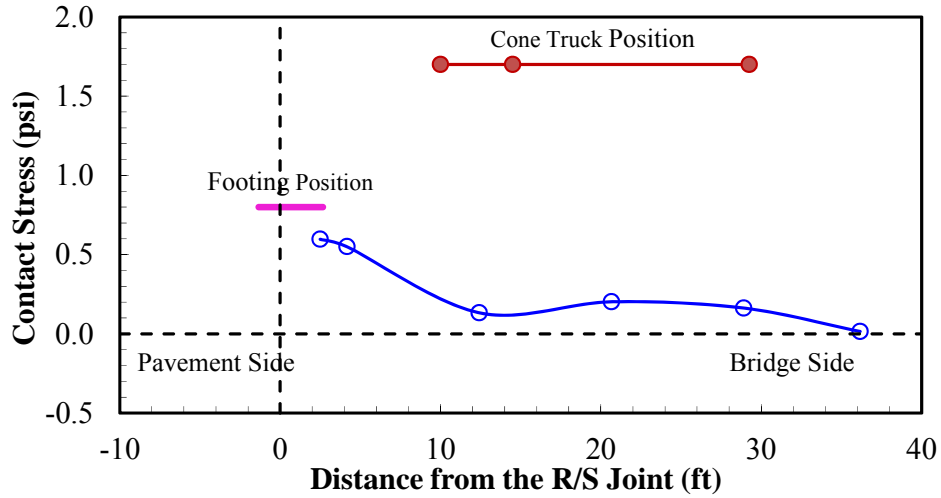


(a) West approach slab

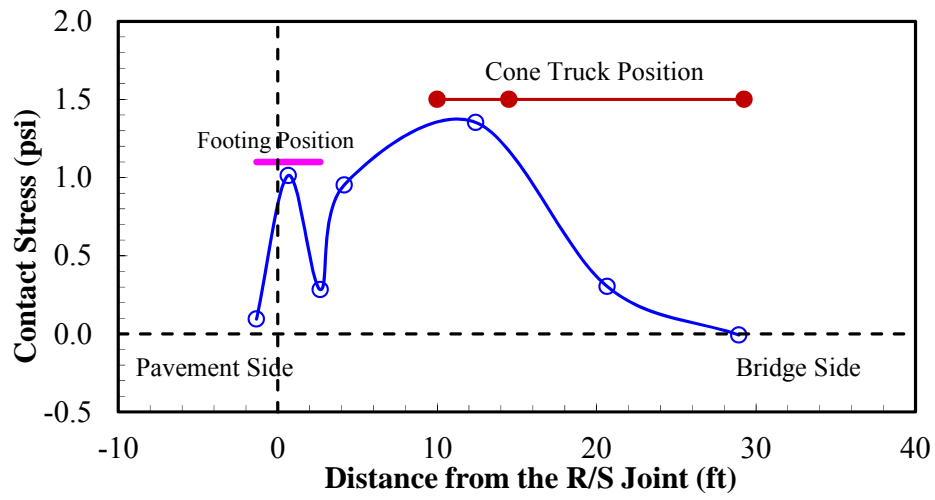


(b) East approach slab

Figure 13
Contact stress between approach slab and embankment when the cone-truck was positioned at Location 5 (October 2009)



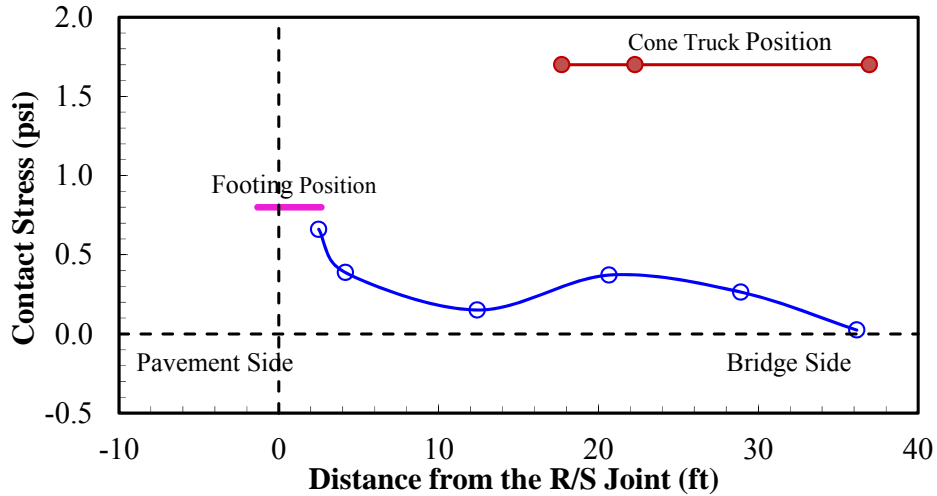
(a) West approach slab



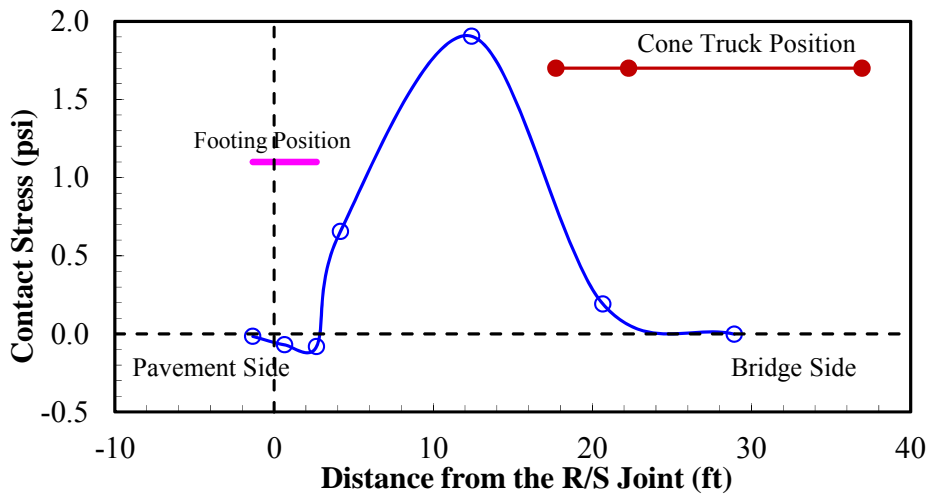
(b) East approach slab

Figure 14

Contact stress between approach slab and embankment when the cone-truck was positioned at Location 3 (March 2011)



(a) West approach slab



(b) East approach slab

Figure 15

Contact stress between approach slab and embankment when the cone-truck was positioned at Location 5 (March 2011)

Internal Strain of the West Approach Slab

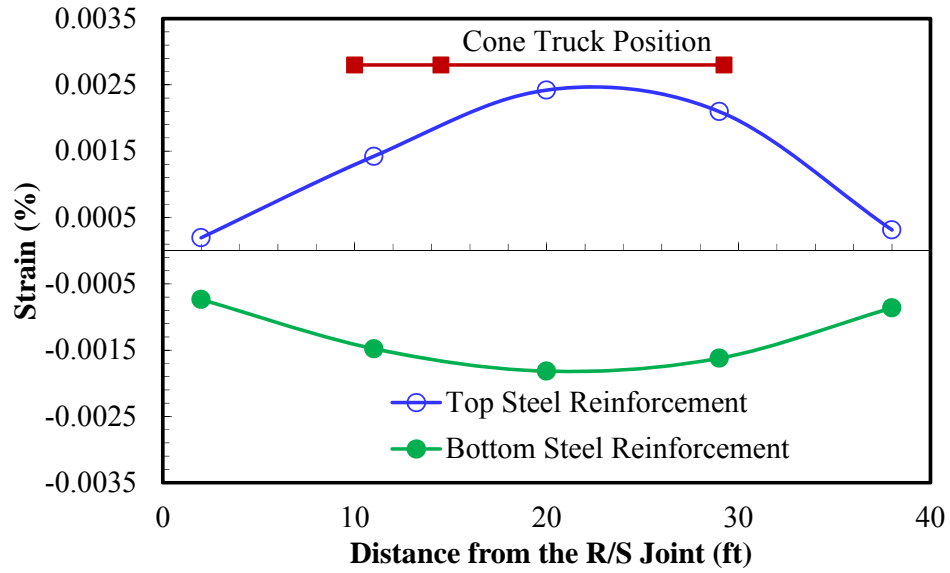
Figure 16a and 16b show the distribution of internal strains in the west approach slab that were measured in October, 2009 and March, 2011 load test, respectively, when the large cone truck was positioned at the center of the slab, as shown in Figure 8c. The compressive strains here are taken as positive. As indicated in the figure, tensile strains were developed at

the bottom of the slab, while compressive strains were developed at the top of slab as a result of the cone truck load with the position shown in the figure. Higher strains were registered during the second static load test due to the fact that the west approach slab lost most of its support from the embankment soil at that time.

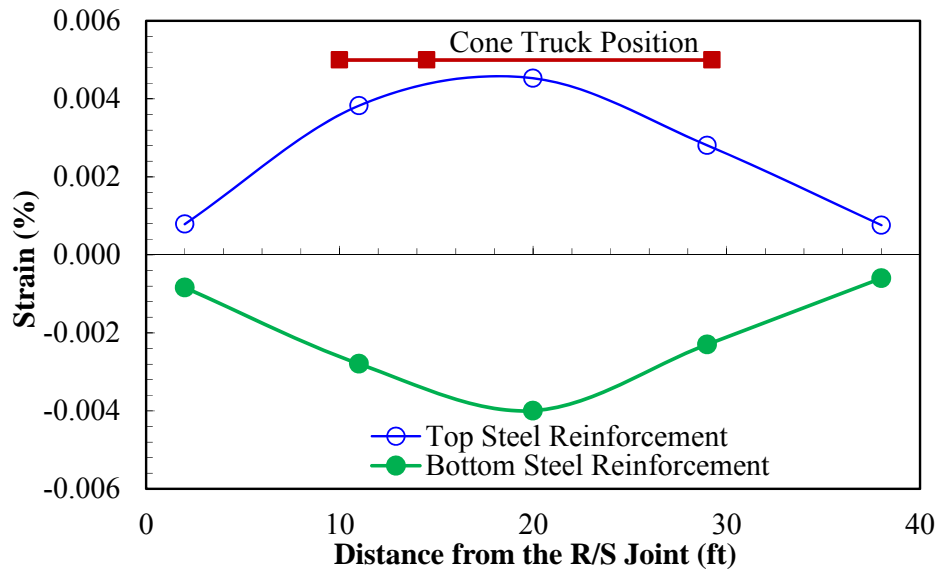
Stress Distribution within Reinforced Soil Foundation

Figure 17a and 17b present the variations of stress distributions within the reinforced soil foundation measured during the first static load test (October, 2009) when the rear wheels of the rear tandem axles of the large cone truck were located at the roadway pavement side of the R/S joint, as shown in Figure 8a. As can be seen from the figure, the pressures registered by the pressure cells were the largest at the point between the rear tandem axles with a position closer to the front wheels of the rear tandem axles. This can be explained by the fact that the rear wheels of the rear tandem axles transferred the loads to the soil through two interfaces (pavement to footing, then to soil), while the front wheels of the rear tandem axles distributed the loads to the soil directly through the slab. As such, the truck loading from the rear wheels of the rear tandem axles would be distributed over a larger area of soil than that from the front wheels of the rear tandem axles.

The variations of stress distributions within the reinforced soil foundation measured during the second static load test (March, 2011) were shown in Figure 18a and 18b for 3 ft. and 6 ft. below the footing, respectively. As compared to the first static load test, the largest pressure registered by the pressure cells was shifted to the point below the center of the footing during the second static truck load test and in addition, the magnitude of pressure was increased. This indicates that more truck load was transferred from the approach slab to the reinforced soil foundation during the second static truck load test through the strip footing (sleeper slab). This further confirms that the west approach slab already lost most of its contacts and supports from the embankment soil by March 2011.

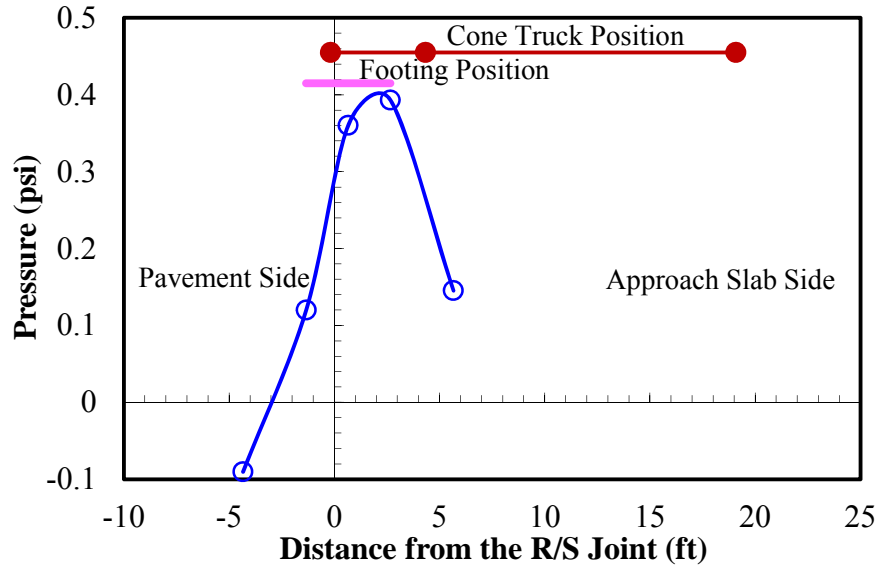


(a) October 2009

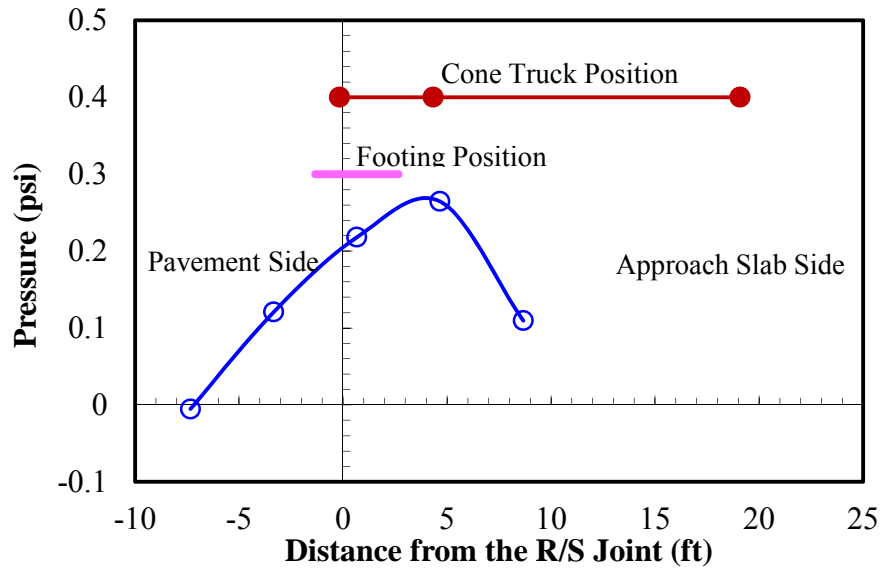


(b) March 2011

Figure 16
Internal strain distributions within the approach slab



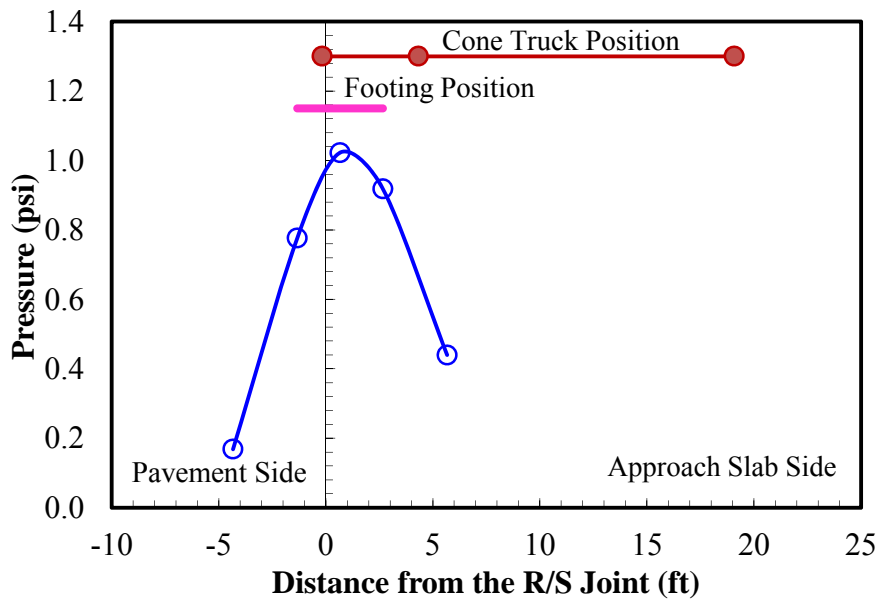
(a) 3 ft. below the footing



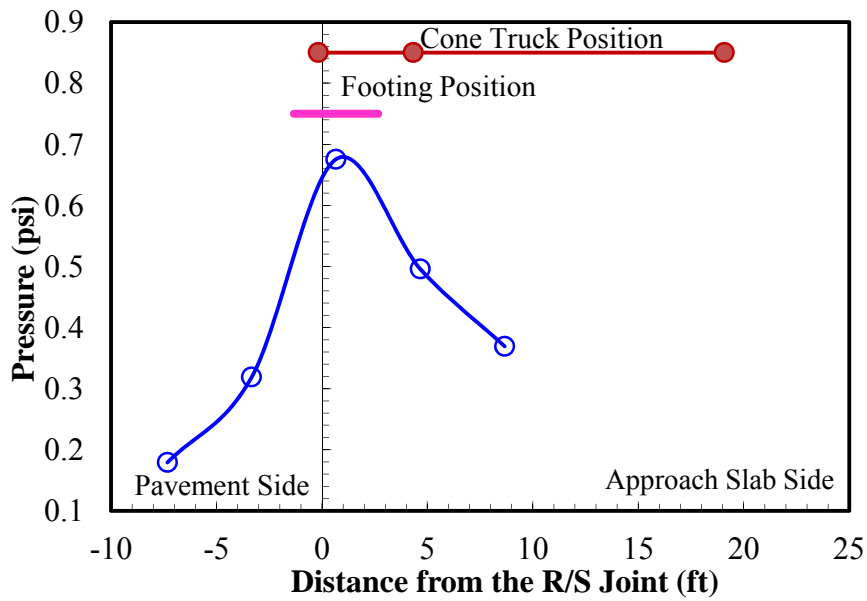
(b) 6 ft. below the footing

Figure 17

Stress distributions within the reinforced soil foundation (October 2009)



(a) 3 ft. below the footing



(a) 6 ft. below the footing

Figure 18

Stress distributions within the reinforced soil foundation (March 2011)

Strain Distribution along the Geogrid

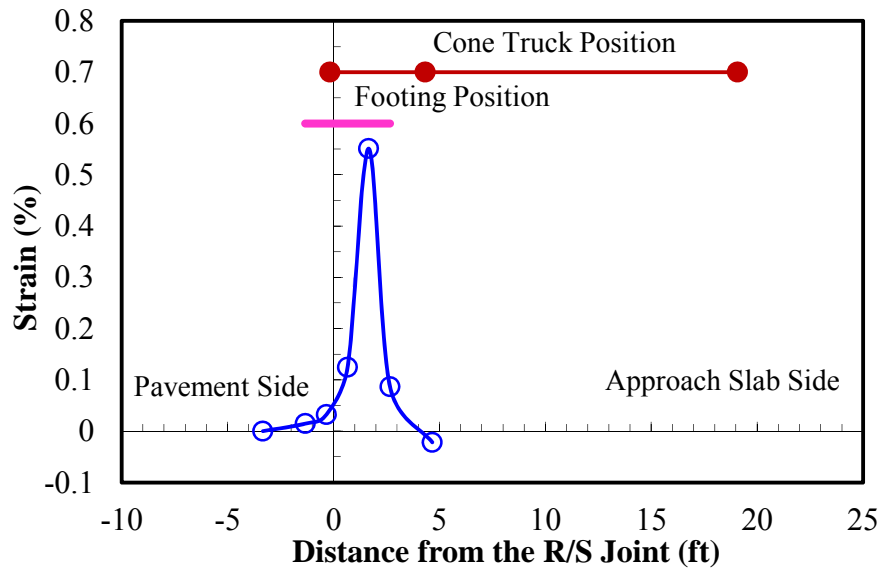
Figure 19a and 19b present the variations of strain measurements along the geogrid reinforcements during the first static load test when the rear wheels of the rear tandem axles of the cone truck were located at the roadway pavement side of the R/S joint, as shown in Figure 8a. The measured tensile strain was the largest at the point between the rear tandem axles, which is consistent with the location of the maximum measured pressure within the reinforced soil foundation (Figure 17a and 17b). The maximum measured strains were 0.55% for the geogrid located 1 ft. below the footing and 0.13% for the geogrid located 3 ft. below the footing. Both maximum measured strains are significantly below the 2% strain, which is the value normally published by manufacturers and usually used for design.

The variation of strains measured along the geogrid reinforcements during the second static load test (March, 2011) was shown in Figure 20a and 20b for the geogrid placed 1 ft. and 3ft. below the footing, respectively. Similar to the measured pressure distribution within the reinforced soil foundation (Figure 18a and 18b), the largest measured tensile strain was also shifted to the point below the center of the footing, and was also increased in magnitude during the second static truck load test. The maximum measured strains (Figure 20a and 20b) are still way below the manufacturer's published 2% strains.

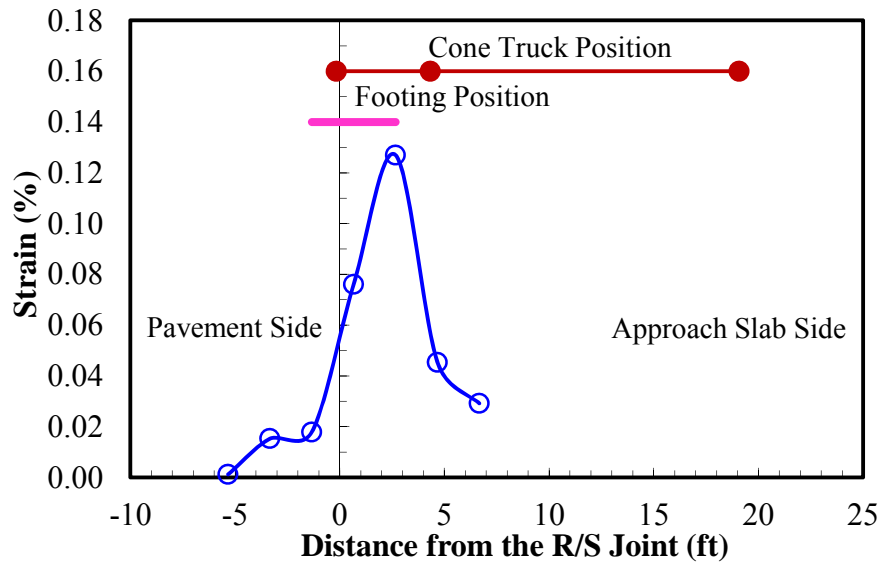
International Roughness Index (IRI) Measurement

Continuous IRI measurements were taken from 20 ft. behind the roadway pavement/west (east) approach slab joint (R/S joint) all the way to the 20 ft. beyond the roadway pavement/east (west) approach slab joint (R/S joint). Three repeated profile testing runs were performed on both the eastbound and the westbound lanes. Figure 21 shows the roughness profiles for the left wheelpath obtained for three repeated runs on the westbound lane. The three roughness profiles show good agreement. This implies that minor variations in the wheelpath during profiling did not affect IRI very much. The average roughness profiles of the left and right wheel paths of three repeated runs are presented in Figure 22 for both the eastbound and the westbound lanes. The two average roughness profiles show strong agreement, except at R/S and S/D joints of east approach slab. IRI values at R/S and S/D joints of east approach slab, shown in this figure, are 1,267 in./mi. and 1,279 in./mi. for westbound, and 685 in./mi. and 467 in./mi. for eastbound. This indicates that the measured IRI values were higher when the profiler system approaches the bridge than when the profiler system leaves the bridge. The difference in the IRI values may be because of the faulting at the joints, as shown in Figure 23, making the profiler system bumping up when approaching the bridge and bumping down when leaving the bridge. The two average roughness profiles also show better performance of west approach slab with much lower IRI values, which is

consistent with the visual observations shown in Figure 23. The average 25-ft continuous IRI profiles also show that the maximum 25-ft IRI values of the east approach slab, on March 24, 2011, were 360 in./mi. and 530 in./mi. for eastbound (approach slab) and westbound (leave slab), respectively. These values increased to 540 in./mi. and 700 in./mi. on January 15, 2014. Meanwhile, the maximum 25-ft IRI values of the west approach slab remained almost constant (around 300 in./mi. during this period).



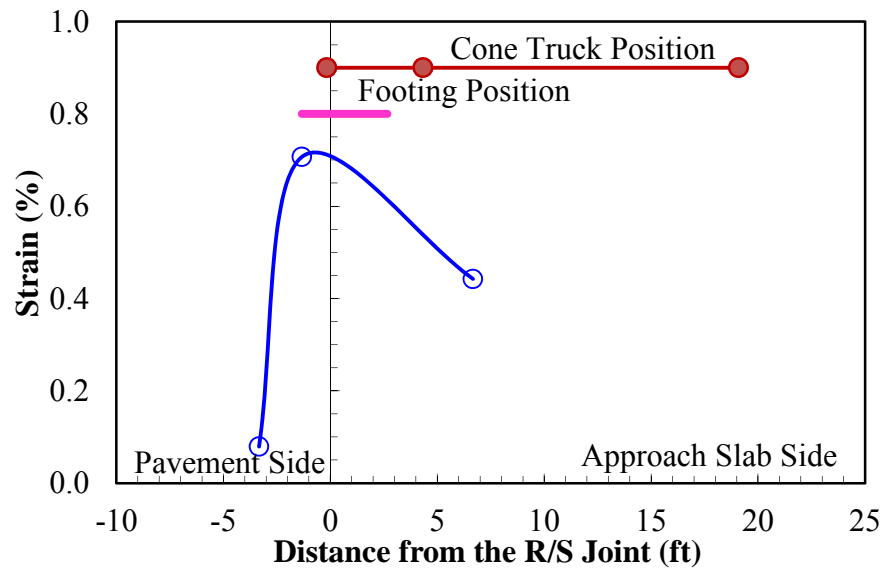
(a) 1 ft. below the footing



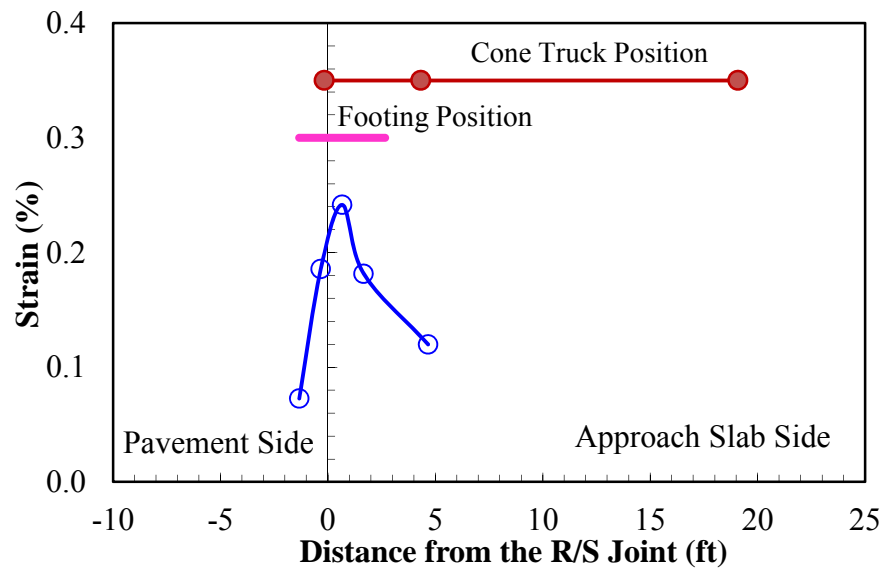
(b) 3 ft. below the footing

Figure 19

Strain distributions along the geogrid (October 2009)



(a) 1 ft. below the footing



(a) 3 ft. below the footing

Figure 20

Strain distributions along the geogrid (March 2011)

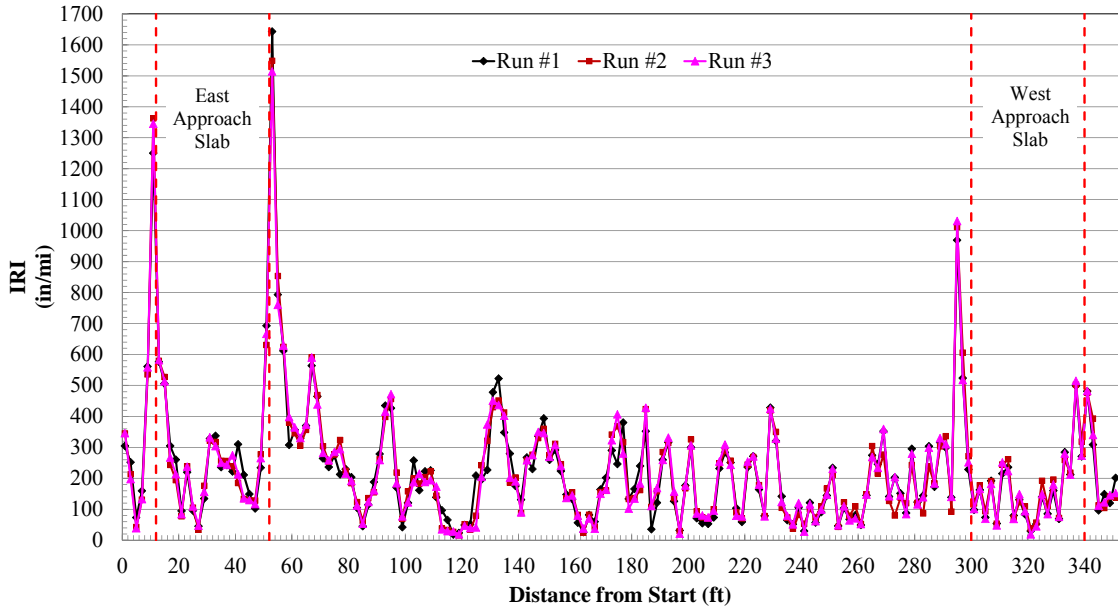


Figure 21
Roughness profiles for three runs along the left wheelpath on the westbound lane

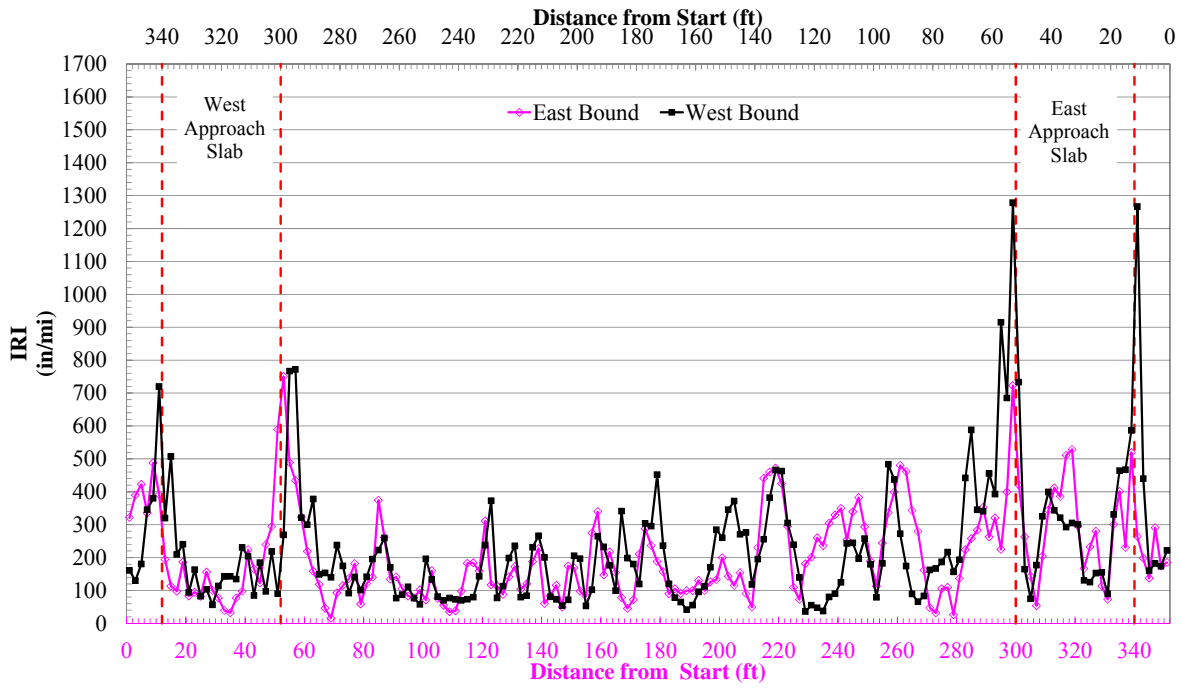


Figure 22
Average roughness profiles at the eastbound and the westbound lanes



(a) West approach slab



(b) East approach slab

Figure 23
Photos of R/S joints

Embankment Settlement

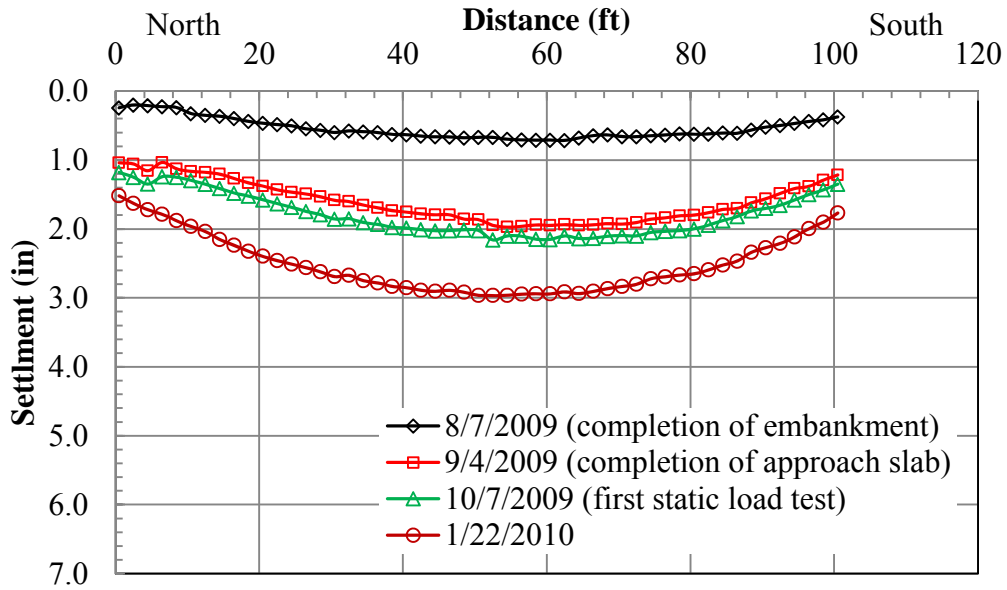
Field Measurement

The field-measured settlement profiles from the horizontal inclinometers are shown in Figure 24a and 24b for east and west embankment side, respectively. The figure shows that significant settlement occurred from August 7, 2009 to September 4, 2009, which corresponds to the time period between the completion of embankment and the completion of approach slab. This figure also indicates very small settlement developed from September 4, 2009 to October 7, 2009, which corresponds to the time period from the completion of approach slab to the first static truck loading test. This measurement is consistent with the contact stress measurements shown in Figure 12a and 11b during the first static truck loading test. Despite insignificant settlement measured from September 4, 2009 to October 7, 2009, the settlement still kept gradually increasing after the completion of approach slab, as demonstrated by the last settlement profile measured on January 22, 2010. This observation agrees with the contact stress measurements during the second static loading test, as shown in Figure 14.

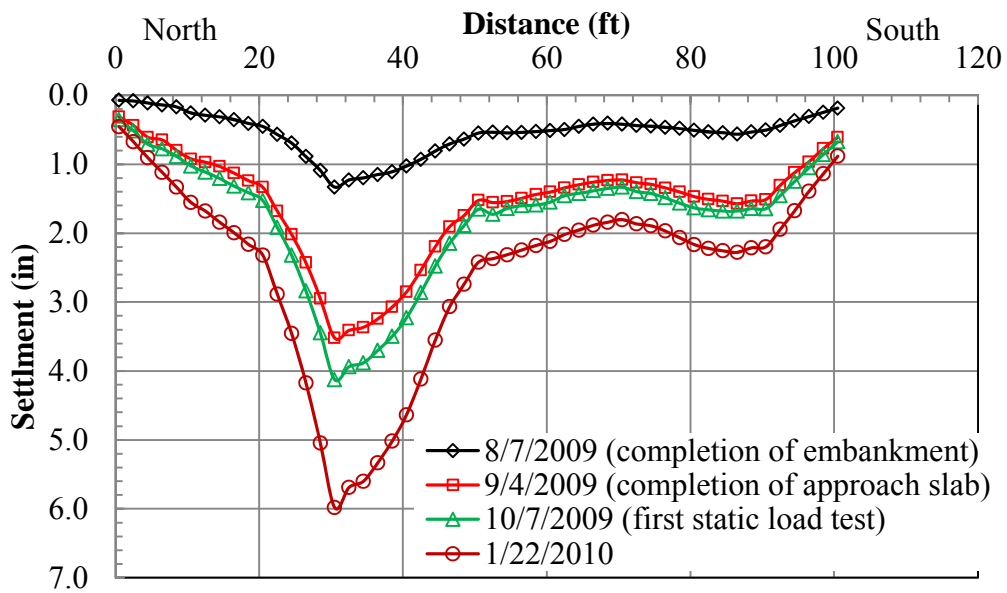
Settlement Prediction

The PCPT data obtained on each embankment site were used to estimate the constrained modulus, M , using the Sanglerat method [14] and Abu-Farsakh correlation ($M=3.15q_t$) [3], with q_t representing the average q_t value of the soil layer. The PCPT estimated constrained modulus along with those obtained from 1-D consolidation tests are depicted in Figure 25a. The figure shows that both Sanglerat and Abu-Farsakh methods have close estimations of the in situ constrained moduli, which are generally larger than the laboratory measured values, especially in the upper 15 ft.

The vertical coefficients of consolidation, c_v , were obtained using the Teh and Houlsby interpretation method from dissipation test results as described by equations 5-7 [16]. The Rigidity indices were determined using the laboratory UU and k_o -CU test results. Coefficient of consolidation is difficult to determine accurately in nature. The PCPT estimated vertical coefficients of consolidation generally agree well with the laboratory measured values (Figure 25b).



(a) East embankment

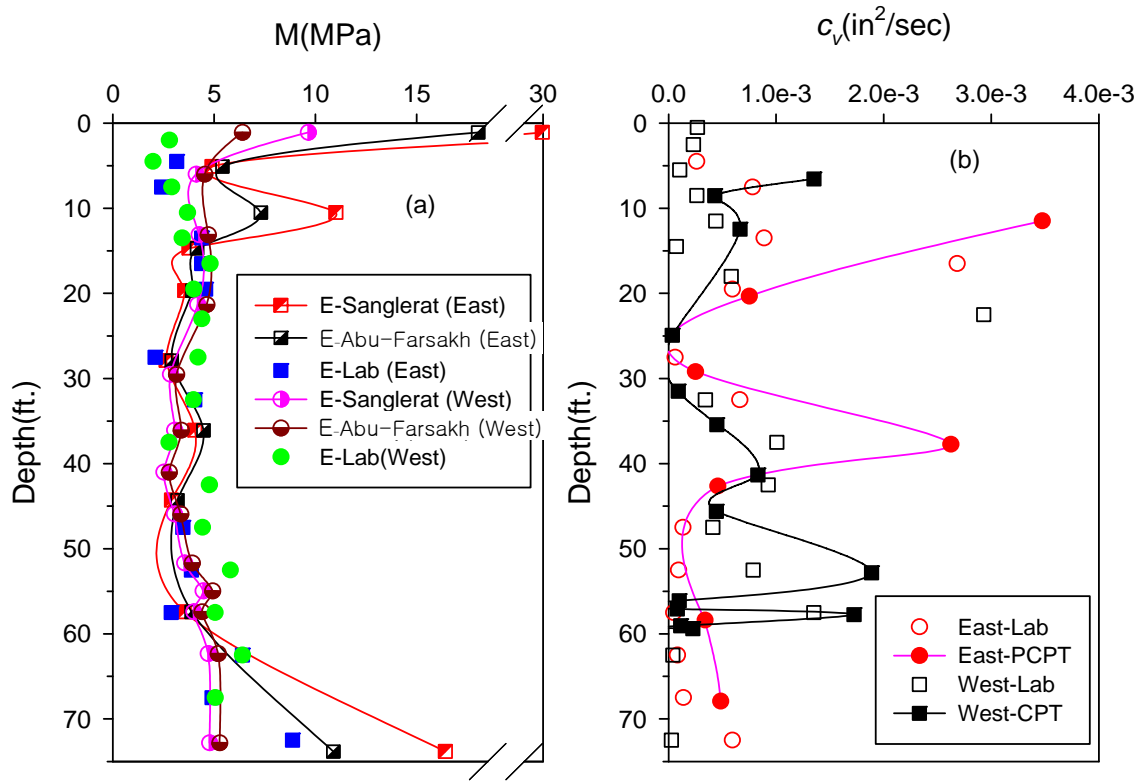


(b) West embankment

Figure 24
Measured settlement profile

The settlement calculation of the Courtableau Bridge embankments was performed based on the results of laboratory tests on retrieved in-situ samples and the PCPT test data. The embankment additional surcharge was obtained as the height difference between the new embankment and the existing embankment as indicated in Figure 10. Stress induced by the applied embankment surcharge ($\Delta\sigma$) is calculated using a MatLAB coding based on the concept of vertical stress distribution due to embankment loading [18]. The 1-D consolidation test results conducted in the laboratory were used for settlement calculation as indicated by “-Lab” shown in Figure 26a and 26b for the east and west embankments, respectively. The subsurface soil properties and the PCPT and the dissipation test results were presented earlier. The constrained modulus and vertical coefficient of consolidation shown in Figure 25 were also used for settlement calculations. The PCPT-predicted settlements (using Sanglerat and Abu-Farsakh correlations of M) were compared with the laboratory-calculated settlement and the field-measured settlement from the horizontal inclinometers as shown in Figure 26. The figures show that the Abu-Farsakh PCPT interpretation method predicted the total consolidation settlement better than the Sanglerat PCPT method and the laboratory method. The settlement predicted from the laboratory tests results in the largest settlement prediction. The Sanglerat method resulted settlements are slightly larger than the settlement obtained by the Abu-Farsakh method.

The accurate prediction of the rate of embankment settlement is very important to geotechnical engineers for better planning the extent of the preloading period needed to overcome the majority of consolidation settlement. The rates of consolidation settlement underneath the center of the embankments, predicted from the laboratory parameters and the PCPT dissipation tests using the Teh and Houlsby interpretation method, are presented in Figure 27a and 27b for the east and west embankments, respectively [16]. The figure indicated that although the predicted magnitudes of settlement from laboratory and PCPT methods vary from the actual field measurements, the PCPT estimated rate of consolidation settlement from dissipation tests matches fairly well with the field monitoring.

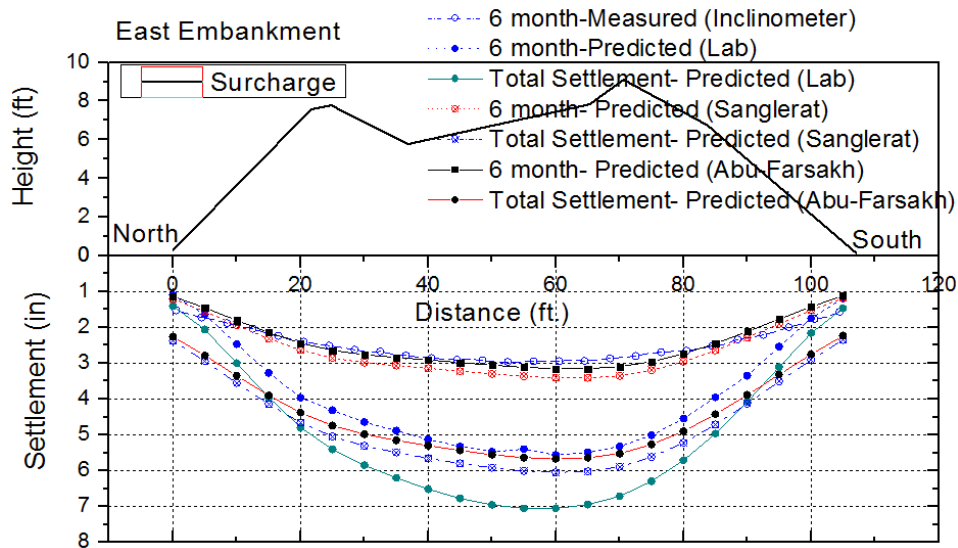


(a) Constrained modulus

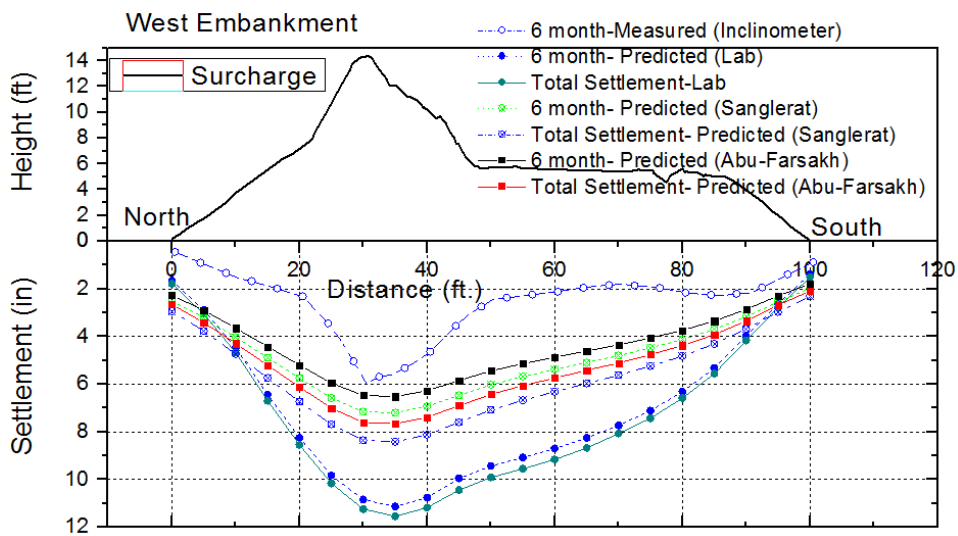
(b) Coefficient of Consolidation

Figure 25

Comparison of constrained modulus and coefficient of consolidation

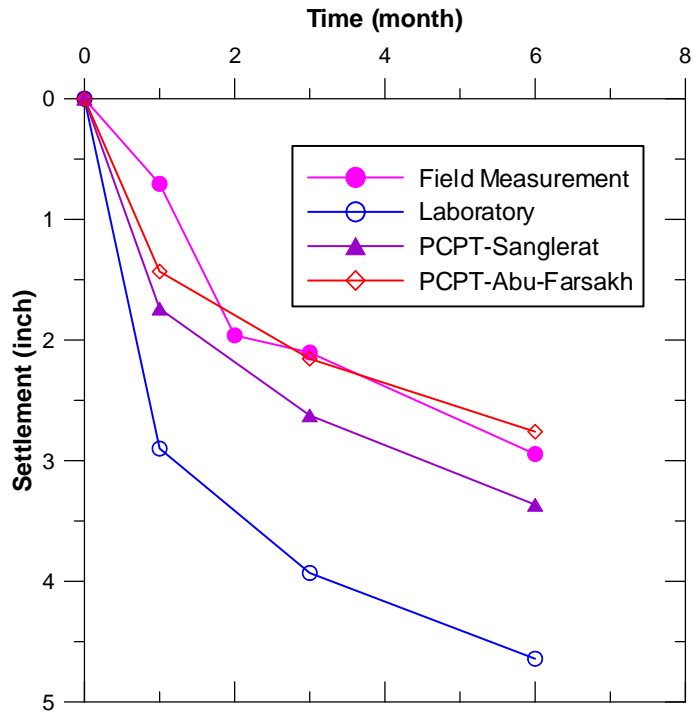


(a) East embankment

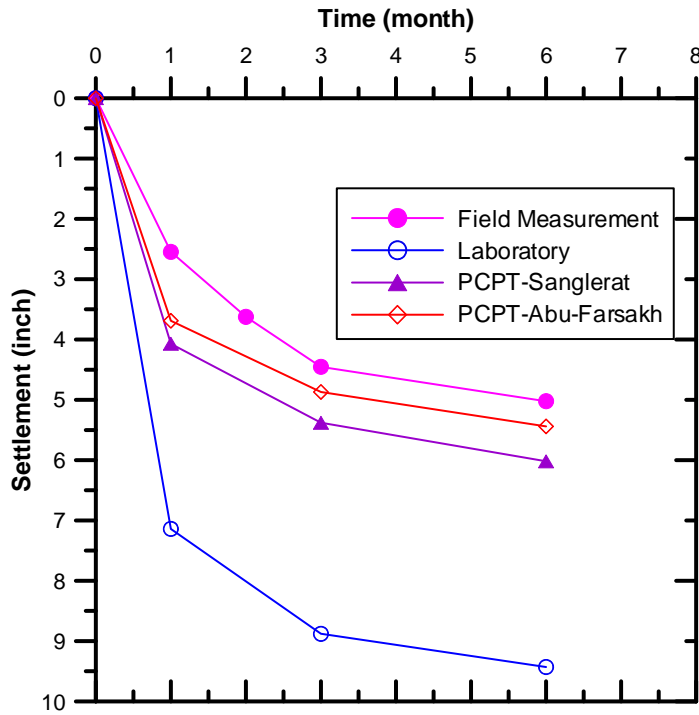


(b) West embankment

Figure 26
Comparison of Settlement Prediction



(a) East embankment



(b) West embankment

Figure 27
Rate of consolidation settlement

SUMMARY AND CONCLUSIONS

The bump that frequently develops at the end of the bridge is considered one of the major national bridge maintenance problems that challenge most DOT engineers. To solve this problem, the DOTD has launched a major effort by conducting two research studies, which recommended changing the design of approach slabs through increasing its rigidity (EI) and the use of geosynthetics to reinforce the soil below the strip footing that supports the slab weight and traffic loads at the roadway pavement/approach slab joint (R/S joint) [1, 2]. The Bayou Courtableau Bridge, as part of Louisiana Highway 103 in St. Landry Parish, was used as a demonstration project to validate and verify the findings and design recommendations developed in the previous research projects [1, 2]. The west approach slab was designed using the new design methodology with a slab thickness of 16 in.; while the east approach slab was designed using the traditional design method with a slab thickness of 12 in.. The geosynthetic reinforced soil below the strip footing was designed according to the methodology proposed in a previous study [2]. The pavement end side of the approach slab was supported by a 4.0-ft. wide strip footing with the soil underneath it reinforced by six geogrid layers placed at a vertical spacing of 12 in. The approach slabs were instrumented with pressure cells placed underneath the slabs and footings, strain gauges along the geogrid reinforcements, and sister-bar strain gauges within the west concrete slab. The performance of the new approach slab design (west approach slab) was investigated by performing two static load tests through positioning a 20-ton weight truck at strategic locations on the slab. The deformation and internal stresses of the concrete slab, the contact stresses between the slab and embankment soil, the stress distributions within the reinforced soil foundation, and the strain distributions along geogrids, were monitored during the tests. The magnitude and rate of settlements of the two embankment sides at the Bayou Courtableau Bridge site were also monitored during and after the construction, and the results were compared with the laboratory calculated settlements and the PCPT-based settlement prediction methods. Based on the outcome of the study, the following findings and conclusions are shown:

- The west approach slab of the Bayou Courtableau Bridge, with the new design method, retained its contacts and supports from the embankment soil during the first static load test (at the time when the bridge was ready for traffic). However, during the second static load test (after about a year and half), the west approach slab lost most of its supports from the embankment soil. The maximum measured contact pressure underneath the west approach slab decreased from 1.5 psi (during first static test) to 0.5 psi (during second static test); while at the same time the pressure increased underneath the footing mainly due to load transfer caused by increased slab

rigidity. On the other hand, the east approach slab, with the standard design method, showed slightly gradual loss of its contacts from the embankment soil starting from bridge abutment side towards the pavement side. The maximum measured contact pressure underneath the east approach slab increased from 1.1 psi (during first static test) to 1.4 psi (during second static test).

- The internal strain distributions within the west approach slab show that the top of the slab is in compression, while the bottom of the slab is in tension (as expected). The maximum measured compression strain (after one and a half years) for the top steel reinforcement was about 0.004%, and the maximum measured tension strain for the bottom steel reinforcement was also about - 0.004%. No measurements from the east approach slab are available for comparison.
- The maximum measured strains in the geogrid due to 20-ton truck loading were considerably lower than the 2% strain (max strain at 1 ft. below footing < 1 %), which is the typical design strain value published by geosynthetic manufacturers.
- The average 25-ft continuous IRI profiles demonstrated much better performance of the new approach slab system (west approach slab) compared to the traditional design method (east approach slab) with much lower IRI values. The maximum 25-ft IRI values of the east approach slab increased from 360 in./mi. for eastbound and 530 in./mi. for westbound on March 24, 2011, to 540 in./mi. for eastbound and 700 in./mi. for westbound on January 15, 2014. Meanwhile, the maximum 25-ft IRI values of the west approach slab remained almost constant (around 300 in./mi.) during this period.
- The improved performance of the new approach slab system on the west approach slab (increasing slab rigidity, EI, and using geosynthetics to reinforce the soil below the strip footing) was clearly demonstrated and visually observed in Bayou Courtableau Bridge demonstration project after a year-and-a-half monitoring period.
- The Bayou Courtableau Bridge case demonstrated the effectiveness of using geosynthetic reinforced soil to support strip footing in terms of increasing the bearing capacity of the embankment soil and redistributing the applied vertical load.
- The comparison between the PCPT-based settlement prediction methods and the field measurements clearly showed that the PCPT and dissipation data were able to reasonably estimate the magnitude and rate of consolidation settlement.

RECOMMENDATIONS

1. More demonstration field projects are needed to further verify the superior performance of the proposed new approach slab design system, especially in cases where excessive embankment settlements are expected.
2. For future demonstrations, creating a small gab between the approach slab and embankment soil (no contact) to demonstrate the performance of new approach slab systems under worst scenario condition is recommended.
3. It is recommended to continue monitoring the performance of the new and traditional approach slab systems at the Bayou Courtableau Bridge by periodically conducting IRI measurements.

ACRONYMS, ABBREVIATIONS, AND SYMBOLS

AASHTO	American Association of State Highway and Transportation Officials
CPT	Cone Penetration Test
CU	Consolidated undrained
FHWA	Federal Highway Administration
IRI	International Roughness Index
LA	Louisiana
DOTD	Louisiana Department of Transportation and Development
LL	Liquid Limit
LTRC	Louisiana Transportation Research Center
MC	Moisture Content
OCR	Overconsolidation Ratio
PCPT	Piezocone Penetration Test
PL	Plastic Limit
RSF	Reinforced Soil Foundation
R/S	Roadway Pavement/Approach Slab
S/D	Roadway Pavement/Bridge Deck
USCS	Unified Soil Classification System
UU	Unconsolidated undrained

REFERENCES

1. Cai, C.S., Voyiadjis, G. Z., and Shi, X. (2005). "Determination of interaction between bridge concrete approach slab and embankment settlement," Final Report, Louisiana Transportation Research Center (LTRC), Louisiana Department of Transportation and Development (DOTD), Baton Rouge, LA, Report No. FHWA/LA.05/403, 150 p.
2. Abu-Farsakh, M. Y., Chen Q., and Yoon S. (2007). "Use of Reinforced Soil Foundation (RSF) to Support Shallow Foundation," Final Report, Louisiana Transportation Research Center, Baton Rouge, LA, Report No. FHWA/LA. 08/424 195 p.
3. Abu-Farsakh, M. Y. (2004). Evaluation of Consolidation Characteristics of Cohesive Soils from Piezocone Penetration Tests. Louisiana Transportation Research Center Baton Rouge, LA, Report: 386, pp. 106.
4. Briaud, J.L., James, R.W., and Hoffman, S.B. (1997). "Settlement of bridge approaches (the bump at the end of the bridge)," NCHRP Synthesis 234, Transportation Research Board, National Research Council, Washington D.C., 75 p.
5. Puppala, A.J., Saride, S., Archeewa, E., Hoyos, L.R., and Nazarian, S. (2009). "Recommendations for design, construction, and maintenance of bridge approach slabs: synthesis report," Final Report, Texas Department of Transportation, Austin, TX, Report No. FHWA/TX-09/0-6022-1, 186 p.
6. Martinez, M. (2009). "The rideability of a deflected bridge approach slab," Final Report, Louisiana Transportation Research Center (LTRC), Louisiana Department of Transportation and Development (DOTD), Baton Rouge, LA, Report No. FHWA/LA.09/4457, 60 p.
7. Abu-Faraskh, M. Y., Zhang, Z., and Gautreau, G. (2007). "Evaluating the Deformation Modulus of Cohesive Soils from PCPT for Consolidation Settlement Estimation." Journal of the Transportation Research Board. 2004: 49-59.
8. Chen, Q., 2007. "An experimental study on characteristics and behavior of reinforced soil foundation." PhD dissertation, Louisiana State University, Baton Rouge, USA.
9. Meyerhof, G.G., and Hanna, A.M., 1978. "Ultimate bearing capacity of foundations on layered soils under inclined load." Canadian Geotechnical Journal, Vol. 15, No.4, pp. 565-572.

10. Louisiana Department of Development and Transportation (DOTD). (2004). *Bridge Design Manual*, Louisiana Department of Development and Transportation, Baton Rouge, LA.
11. Zhang, Z., and Tumay, M. T. (1999). "Statistical to Fuzzy Approach Toward CPT Soil Classification." *Journal of Geotechnical and Environmental Engineering*. 125(3): 179-186.
12. Senneset, K., Sandven, R., Lunne, T., By, T., and Amundsen, T. (1988). *Piezocone Tests in Silty Soils*. Proceedings of the International Symposium on Penetration Testing, ISOPT-1, Rotterdam, Balkema Pub.
13. Senneset, K., Sandven, R., and Janbu, N. (1989). "The Evaluation of Soil Parameters from Piezocone Tests." *Transportation Research Record*(1235): 24-37.
14. Sanglerat, G. (1972). *The Penetration and Soil Exploration*. Amsterdam, Elsevier.
15. Kulhawy, F. H., and Mayne, P. H. (1990). *Manual on Estimating Soil Properties for Foundation Design*, Electric Power Research Institute, EPRI.
16. Teh, C. I., and Houlsby, G. T. (1991). "An Analytical Study of the Cone Penetration Test in Clay." *Geotechnique*. 41(1): 17-34.
17. Levadoux, J. N., and Baligh, M. M. (1986). "Consolidation after Undrained Piezocone Penetration. II: Prediction." *Journal of Geotechnical Engineering*. 112(7): 707-726.
18. Poulos, H. G., and Davis, E. H. (1974). *Elastic Solutions for Soil and Rock Mechanics*. New York, John Wiley and Sons, Inc.